4-2016

Failure pressure and fatigue analysis of the API 12F shop welded, flat bottom tanks

Andres E. Rondon Andueza
Purdue University

Graduate School Form
30 Updated 12/26/2015

PURDUE UNIVERSITY
GRADUATE SCHOOL
Thesis/Dissertation Acceptance

This is to certify that the thesis/dissertation prepared

By ANDRES EDUARDO RONDON ANDUEZA

Entitled

FAILURE PRESSURE AND FATIGUE ANALYSIS OF THE API 12F SHOP WELDED, FLAT BOTTOM TANKS

For the degree of Master of Science in Civil Engineering

Is approved by the final examining committee:

Sukru Guzey
Co-chair

Mark Bowman
Co-chair

Ghadir Haikal

To the best of my knowledge and as understood by the student in the Thesis/Dissertation Agreement, Publication Delay, and Certification Disclaimer (Graduate School Form 32), this thesis/dissertation adheres to the provisions of Purdue University's "Policy of Integrity in Research" and the use of copyright material.

Approved by Major Professor(s): Sukru Guzey

Approved by: Dulcy Abraham 04/20/2016

Head of the Departmental Graduate Program Date

FAILURE PRESSURE AND FATIGUE ANALYSIS OF THE API 12F SHOP WELDED, FLAT BOTTOM TANKS

A Thesis

Submitted to the Faculty

of

Purdue University

by

Andres E Rondon Andueza

In Partial Fulfillment of the

Requirements for the Degree

of

Master of Science in Civil Engineering

May 2016

Purdue University

West Lafayette, Indiana

To my beloved wife
Gisela

To my mother
Carmen

For all the love and support they have given me throughout all these years.

ACKNOWLEDGEMENTS

I would like to express my sincere gratitude to my advisor Professor Sukru Guzey for his invaluable support, advice, and friendship throughout the development of this project. My research would not have been possible without his guidance and motivation

I would also like to thank my examination committee members, Professor Mark Bowman, and Professor Ghadir Haikal for serving on my defense committee and for their support and advice throughout my time at Purdue.

Additionally, I would like to gratefully acknowledge the support from the American Petroleum Institute, Committee on Refinery Equipment, Subcommittee on Aboveground Storage Tanks, Work Group on 12 Series documents, and Task Group on 12F Pressure Research Project. I would also like thank to George Morovich, Mark Baker, David Nadel, Philip Myers, Kieran Claffey, and Nathaniel Wall for fruitful discussion and support throughout the study.

TABLE OF CONTENTS

Page

LIST OF TABLES

Table Page

LIST OF FIGURES

Figure Page

ABSTRACT

Rondon Andueza, Andres E M.S.C.E., Purdue University, May 2016. Failure Pressure and Fatigue Analysis of the API 12F Shop Welded, Flat Bottom Tanks. Major Professor: Sukru Guzey.

This study investigates the failure pressure on the API 12F shop welded steel tanks and performs a fatigue evaluation to estimate the permissible number of pressure cycles for these equipment. Four different analyses were carried out on more than 350 finite element models to determine various failure pressure modes of these storage tanks. An elastic analysis considering potential buckling modes was developed to determine the yielding pressure of the tanks. The redistribution of stresses due to inelastic deformations and plastic collapse were evaluated through an elastic-plastic stress analysis considering the plastic hardening of the material. A wind load analysis was performed to evaluate the stress levels at all regions of the tank and estimate the uplift deformations. Moreover, the increase of the design pressure was investigated regarding the stress levels and bottom uplift. Additionally, an elastic stress analysis following the ASME Boiler & Pressure Vessel Code Section VIII, Division 2, Design-by-Analysis rules was implemented to determine the fatigue life of the storage tanks. This research provides engineering calculations to evaluate the current design of the API 12F tanks and the design internal pressures guaranteeing a safe performance of the equipment.

CHAPTER 1. INTRODUCTION

1.1 Thesis Background

The API specification 12F is intended to provide material, design, fabrication, and testing requirements for a list of standard shop-built, flat bottom steel storage tanks. These tanks are often used in the exploration and production phases of the oil and gas industry and they are fabricated, completely furnished in accordance to the need of the purchaser, and shipped ready for installation in the field.

The motivation of this research is to investigate the behavior of shop-welded tanks under different load cases. The American Petroleum Institute, Committee on Refinery Equipment, Subcommittee on Aboveground Storage Tanks (API SCAST) identified the need to determine the failure modes for tanks built to API 12F. Thus, API 12F Flat Bottom Tanks Failure Pressure Study (Phase 1) was developed under the API Contract #2015-109646 and presented the research findings in the report #15G06-01 dated November 11, 2015 as well as submitted as a technical paper in the Thin-Walled Structures journal.

The analysis and results obtained in Phase 1 of the mentioned study are summarized in Chapter 2 of this thesis. Based on the conclusions of Phase 1, API SCAST identified the need to further investigate the API 12F Flat Bottom Tanks to determine the fatigue life and perform brittle fracture evaluation of the subject tanks by using established fatigue and fracture mechanics principles.

The fatigue analysis and estimation of allowable pressure cycles of each tank are presented in Chapter 3. The brittle fracture evaluation is not part of the scope of this thesis.

1.2 Objective and Scope

The objective of this study is to determine the various failure pressure modes for shop-welded flat-bottom tanks for oilfield production liquids. Moreover, this investigation aims to perform a fatigue analysis to estimate the minimum number of pressure cycles for each API 12F storage tank.

The scope of the study included: (a) an elastic stress analysis to determine the yielding pressure of the steel tanks, evaluate the relative strength ratio between the roof-to-shell and bottom-to-shell joints, and investigate stress levels and uplift deformations due to the design internal pressure, (b) an elastic buckling mode analysis to estimate potential buckling modes of the tanks, (c) an elastic-plastic stress analysis considering the plastic hardening of the material and non-linear deformations to determine the plastic collapse of the tanks, (d) a wind load analysis on the API 12F shop-welded tank with the greatest height-diameter ratio to show the stress levels at all regions of the tank and uplift deformation, (e) a fatigue analysis to estimate the allowable number of pressure cycles caused by different loading conditions.

1.3 Organization

The thesis contains four chapters. The layout presented in this thesis is as follows:

Chapter 1: background information, objective and scope.

Chapter 2: reviews the investigation developed to evaluate the failure pressure modes of the API 12F shop-welded flat bottom tanks.

Chapter 3: describes the methodology and results of the fatigue evaluation to determine the number of permissible cycles for each steel tank studied.

Chapter 4: summarizes the findings and conclusions presented in this research.

CHAPTER 2. FAILURE PRESSURE OF THE API 12F STORAGE TANKS

2.1 Introduction

API 12F tanks are used for the storage of petroleum production liquids in the upstream, exploration, and production segment of the oil and gas industry. They are shop-fabricated and furnished by the manufacturer ready for the installation. The API 12F specification sets the minimum requirements for material, design, fabrication, and inspection of shop-welded tanks for oilfield production liquids 0. This specification is intended to provide a list of recommended tanks with dimensions and internal pressure capacities for the convenience of purchasers. Moreover, the minimum metal thickness and permissible design pressure suggested by the API 12F are determined to provide tanks of adequate safety and economy.

Failure of aboveground storage tanks can be environmentally threatening and lead to a significant cost impact [2]-[3]. Therefore, engineering calculations in compliance with industry standards and codes have been developed to ensure safe and reliable equipment and designs. Recently, the oil and gas industry identified the need to further investigate the failure pressure modes of the API 12F shop-welded tanks. The purpose of this investigation is to improve the operation performance and evaluate the pressure limits of these tanks. Furthermore, the results of this research is of the interest of tank designers, manufacturers, and purchasers.

The main objective of this study is to develop a stress analysis using finite element models (FEM) to determine the failure pressure on the eleven current API 12F flat bottom tank sizes as well as two proposed new sizes. Since a critical tank problem occurs when the shell-to-bottom joint fails before the roof-to-shell joint [4] and some uncertainty exists regarding the relative strength between both joints [5], the present research evaluates the capacity of the API 12F tanks considering the yielding strength, buckling strength and plastic deformations of the shell-to-bottom and roof-to-shell joint in order to clarify unresolved issues.

The following section provides background information regarding the publications and specifications used for the development of the present study. The mentioned works were used as reference for the construction of the computational models as well as for the validation of the results obtained in the analyses.

2.2 Background Information

2.2.1 API 12F Specification for Shop Welded Tanks for Storage of Production Liquids 0

This specification presents the requirements for shop-welded tanks and provides the oil and gas industry with a series of safe and reasonably economic tanks for the convenience of the manufacturers and purchasers. Moreover, tanks covered in API 12F have been accordingly calculated to assure structural stability and safety while using the minimum metal thickness, welding, and bolting specifications for each size.

API 12F tanks consist of shop-fabricated vertical, cylindrical, aboveground, closed top, welded steel storage tanks, and they are completely fabricated and furnished according to

various standard sizes and capacities for internal pressures stipulated in the specification. The tank bottom shall be flat (Type A) or conical (Type B) while the roof deck shall be self-supported, cone type, with a slope of 1 in. (25.4 mm) in 1 ft. (0.3 m). Diameters of the tanks range from 7 ft. 11 in. (2.4 m) to 15 ft. 6 in (4.7 m), and the heights vary from 8 ft. (4.7 m) to 24 ft. (7.3 m). The working capacity of the tanks range from 72 bbl. (11.4 m^3) to 746 bbl. (118.6 m^3). It can be noted that the dimensions are not particularly large since the purpose of these tanks is to be built in the shop of the manufacturer, transported, and delivered ready for installation in the field.

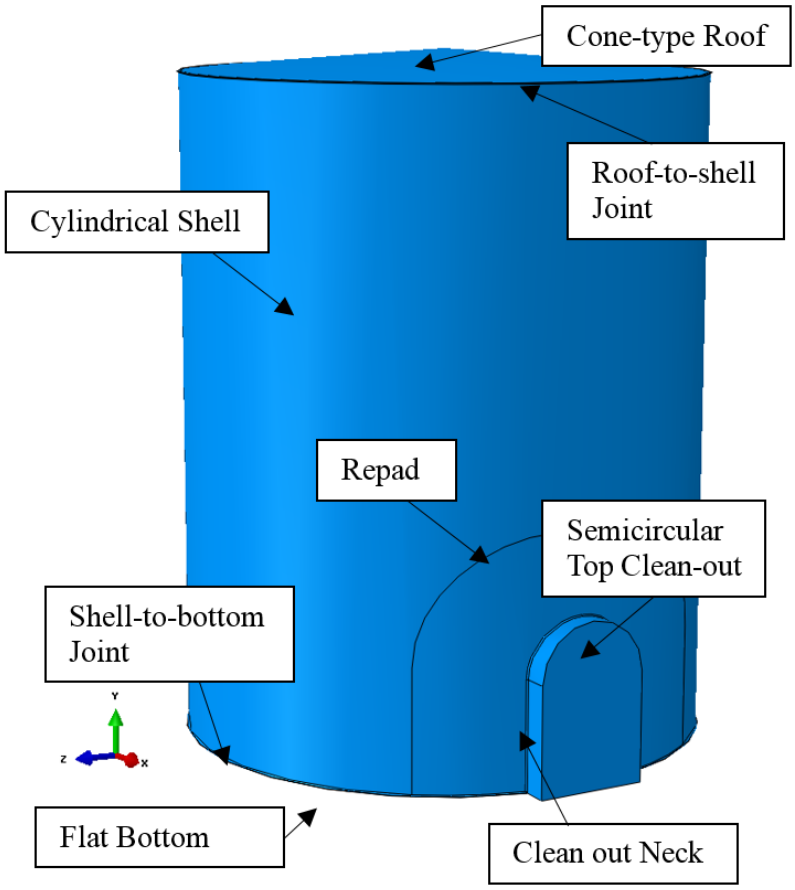

Figure 1. Typical shop-welded, flat-bottom, storage tank with proposed semicircular top clean-out

The materials listed in the specification were selected to provide sufficient strength and reasonable service life. However, if the manufacturer, in agreement with the purchaser, decides to fabricate tanks with higher strength materials, the minimum thickness stipulated in the API 12F shall not be reduced. The thickness of the bottom plates shall be either 1/4 in. (6.4 mm) or 3/8 in. (9.5 mm). Moreover, the thickness of the shell and roof plates shall be the same (3/16 in. (4.8 mm) or 1/4 in (6.4 mm)), except for 15 ft. 6 in. (4.7 m) and larger diameters tanks where the roof shall be 1/4 in. (6.4 mm) nominal unless rafters are provided. Additionally, API 12F tanks shall be furnished with a 36 in. (0.9 m) by 24 in. (0.6 m) extended-neck cleanout. A new 36 in. (0.9 m) high by 24 in. (0.6 m) wide rectangular and semicircular top clean out design has been proposed to avoid local stress concentrations in the proximity of this opening. Typical API 12F shop welded tanks for storage of production liquids with the proposed clean out design is shown in Figure 1.

Table 1 summarizes the standard dimensions and establishes the maximum internal design pressure and vacuum of the eleven current API 12F shop-welded tanks. The limit pressures were obtained from engineering calculations following the minimum metal thickness and bolting specifications for each tank filled with water 0. In addition, the American Petroleum Institute (API) has evaluated to include two new tank sizes: 21 ft. 6 in. (6.6 m) diameter by 16 ft. (4.9 m) high and 15 ft. 6 in. (4.7 m) diameter by 30 ft. (9.1 m) high.

Table 1. Tank Dimensions

Nominal Capacity	**Design Pressure** oz./in² (kPa)	**Approximate Working Capacity**	**Outside Diameter**	**Height**
bbl., m^3	**Pressure, Vacuum**	bbl., m^3	ft-in. (m)	ft., m
90, 14.3	16, ½ (6.9, 0.2)	72, 11.4	7-11 (2.4)	10, 3.0
100, 15.9	16, ½ (6.9, 0.2)	79, 12.6	9-6 (2.9)	8, 2.4
150, 23.8	16, ½ (6.9, 0.2)	129, 20.5	9-6 (2.9)	12, 3.7
200, 31.8	16, ½ (6.9, 0.2)	166, 26.4	12 (3.7)	10, 3.0
210, 33.4	16, ½ (6.9, 0.2)	200, 31.8	10 (3.0)	15, 4.6
250, 39.7	16, ½ (6.9, 0.2)	224,35.6	11 (3.4)	15, 4.6
300, 47.7	16, ½ (6.9, 0.2)	266, 42.3	12 (3.7)	15, 4.6
400, 63.6	16, ½ (6.9, 0.2)	366, 58.2	12 (3.7)	20, 6.1
500, 79.5	16, ½ (6.9, 0.2)	466, 74.1	12 (3.7)	25, 7.6
500,79.5	8, ½ (3.5, 0.2)	479, 76.2	15-6 (4.7)	16, 4.9
750,119.2	8, ½ (3.5, 0.2)	746, 118.6	15-6 (4.7)	24, 7.3

2.2.2 API 937 Evaluation of Design Criteria for Storage Tanks with Frangible Roof Joints [5]

The design procedures and performance of aboveground storage tanks have been influenced by unexpected failures that led to tragic environmental impacts and substantial loss of capital. One of the most undesirable failure modes is the loss of the shell-to-bottom joint of the tank, which not only affects the tank's operation but also can produce major leaks of the content into the ground [6]. Storage tanks with frangible roof joints are designed considering that the roof-to-shell joint will fail before the shell-to-bottom joint in case of excessive internal pressure. The API 650 [7] standard provides the calculation rules for frangible roof tanks and has been a reference of the design of welded tanks for oil storage since it was first published in 1961.

Swenson et al. [8] evaluated the design procedures for frangible roof tanks stated in the API 650, and provided new insights to guarantee the appropriate roof-to-shell joint behavior. The work presented by Swenson was summarized and compiled into the API 937 publication, "Evaluation of Design Criteria for Storage Tanks with Frangible Roof Joints". This publication derived the API 650 design formulation for frangible roofs and compared the failure pressures calculated using these equations with results obtained from the analysis of finite element tank models. Moreover, API 937 concluded that the pressures reported in accordance with the API 650 are significantly lower than the ones computed from the FEA. Additionally, the uplift pressures were calculated using the API 650 rules and FEA, and in this case the results were similar.

The API 937 publication derives the formulation to obtain the maximum design pressure from the Equation (1) and provides Equation (2) to compute the tank's maximum uplift pressure. Also, the publication suggests that the failure pressure is reached when the roof-to-shell joint has yielded. Equation (3) is given to calculate the failure pressure in the tank.

$$P = \frac{8A\sigma_{yield}\tan\theta}{nD^2} + 8\rho_{water}t_h \quad (1)$$

$$P_{max} = \frac{0.245W}{D^2} + 8t_h \quad (2)$$

$$P_f = 1.6\,P - 4.8t_h \quad (3)$$

Where,

P = internal design pressure, in inches of water.

D = tank diameter, in feet.

A = Area resisting the compressive force, in square inches.

σ_{yield} = Compressive yield strength, in pounds per square foot.

θ = Angle between the roof and a horizontal plane at the roof-to-shell junction, in degrees.

n = 1.6. Safety factor

ρ_{water} = Density of water, in pounds per cubic foot.

t_h = nominal roof thickness, in inches.

P_{max} = maximum design pressure, limited by uplift

W = Total weight of the shell and any framing (but not roof plates) supported by the shell and roof, in pounds,

P_f = calculated failure pressure, in inches of water.

1 inch of water = 0.03606 psi

Since the failure mechanism of the tanks with frangible roof joints establishes that the roof-to-shell joint shall fail prior the shell-to-bottom joint, the cross-sectional area of the roof-to-shell joint is limited by Equation (4). For the purpose of this investigation, the cross-sectional area of the roof-to-shell joint was estimated using Figure 2.

$$A = \frac{W}{2\pi\, \sigma_{yield} \tan\theta} \tag{4}$$

The relative strength between the roof-to-shell joint and the shell-to-bottom joint was investigated by Swenson et al. [8]. It was suggested that the liquid level is an important parameter to consider in the failure of tanks due to overpressurization. Swenson identified that the liquid pressure over the bottom of the tank relieves the stresses at that juncture. However, especially for small empty tanks or those with low liquid level, the ratio between the top-yielding pressure and the bottom-yielding pressure is not significant, leading the design to have a small safety factor. Moreover, API 937 suggests that the liquid level to be

used for safety evaluation needs to be stipulated considering that an empty tank has a lower bottom failure pressure and smaller safety factor than a full tank, but an unexpected failure of a full tank can have substantial economic and environmental consequences.

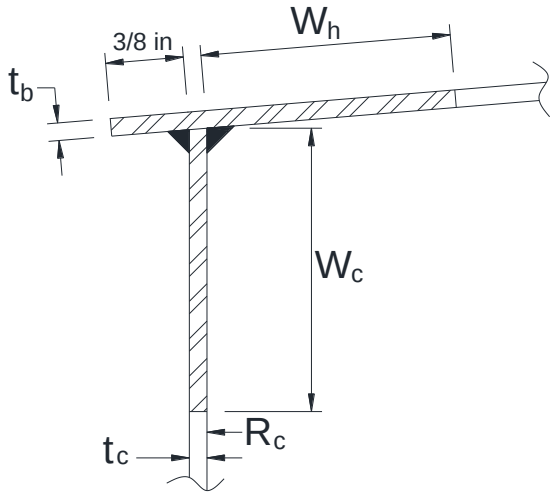

Figure 2. Typical roof-to-shell joint.

2.3 Methodology

Vertical, cylindrical, aboveground, closed top, flat bottom, welded steel storage tanks have been modeled in this research to determine their failure pressure modes as well as study the relative strength between the roof-to-shell and shell-to-bottom joints. The finite element models were built based on the eleven current API 12F shop-welded tanks and the two proposed new sizes. The carbon steel material was considered to be isotropic and elastic-plastic with Young's modulus $E = 2.9 \times 10^7$ psi (2.0×10^5 MPa), Poisson's ratio $\nu = 0.3$, and density $\rho = 490$ lb/ft^3 (7800 kg/m^3). The yield strength (F_y) was taken as 36 ksi (250 MPa), and the ultimate tensile strength was 58 ksi (400 MPa), corresponding to the ASTM A36 steel material [9].

The finite element software ABAQUS version 6.13 [10] was used in this study to perform the stress analysis and determine the failure pressures. Since this research required several FE tank models, quadrilateral shell elements S4R were used to optimize the number of nodes in the simulations and reduce computational time. S4R elements are four-node, doubly curved elements with hourglass control, finite membrane strain, and reduced integration formulation. The mesh size on each tank gradually varies from the center of the shell to the roof and bottom junctures, being coarse in the middle and much finer near the joints. A convergence analysis was performed to evaluate the stresses in the proximity of the welded joints and discard any stress singularity in the computational models. After several iterations and mesh refinements, the convergence of results were verified along the top and bottom joints of the tanks. A typical finite element model is shown in Figure 3.

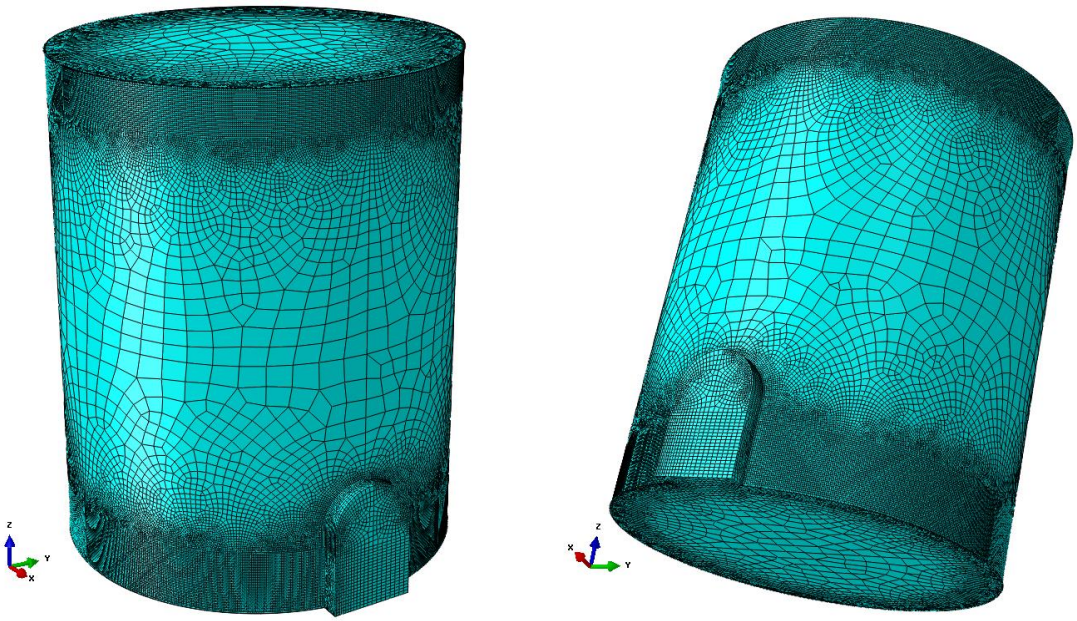

Figure 3. Typical API 12F finite element tank model.

In accordance with the API 12F specification, the flat bottom plate thicknesses used were 1/4 in. (6.4 mm) and 3/8 in. (9.5 mm). Also, the thickness of the cylindrical shell plates were 3/16 in. (4.8 mm) and 1/4 in. (6.4 mm) The roof design was cone-type with a slope of 1 in. (25.4 mm) in 1 ft. (0.3 m), and the plate thicknesses were the same as the shell plates. Additional structural supports in the form of rafters were included in the larger diameter tank models when 3/16 in. (4.8 mm) thick roof plates were used. The models assumed that the rafters were welded to the cylindrical shell and supported by a center column. Moreover, the roof deck was not attached to the rafters. Eight and ten C6x8.2 beam shapes were used for the 15 ft. 6 in. (4.7 m) and 21 ft. 6 in. (6.6 m) diameter tanks, respectively, and a 6 in. (150 mm) standard pipe was assigned to the central column. The center ring plate had a thickness of 1/4 in. (6.4 mm). A typical rafter configuration can be observed in Figure 4.

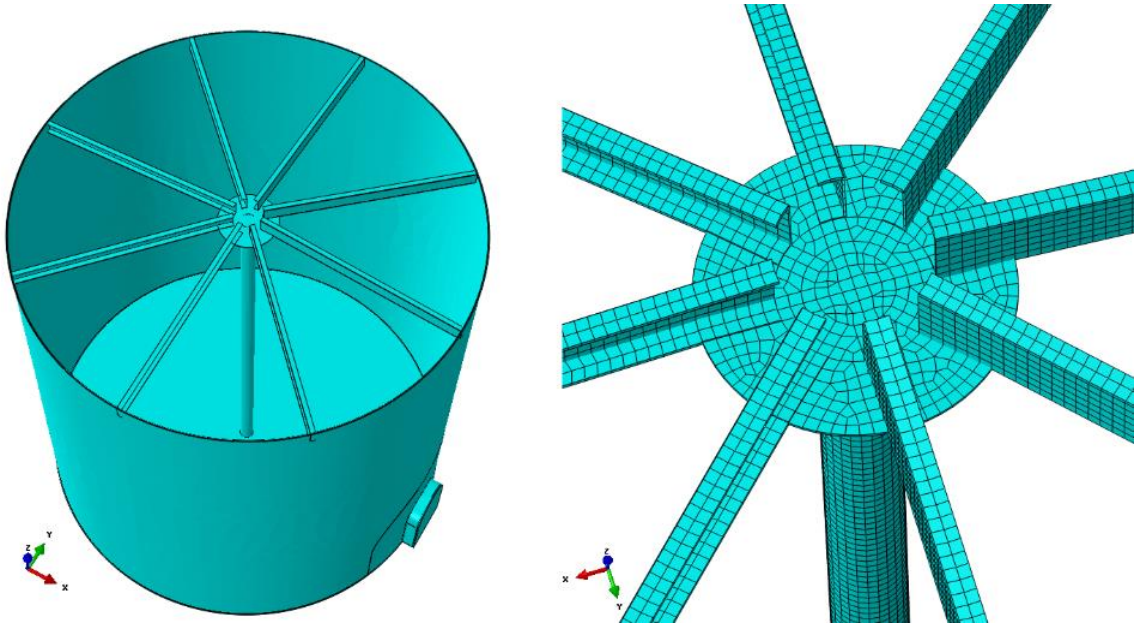

Figure 4. Typical rafter configuration.

The flat bottom and the tank roof had a chime projection of 3/8 in. (9.5 mm) measured from the outer surface of the shell. The non-flanged shell-to-bottom joint included full-fillet welds on the inside and outside surfaces of the tank's shell, and the roof-to-shell was welded with a maximum 3/16 in. (4.8 mm) continuous fillet weld. The computational models of the welded joints were built following the methodology presented by Niemi et al. [11] as shown in Figure 5. A 36 in. (0.9 m) high by 24 in. (0.6 m) wide rectangular and semicircular top clean-out was modeled as shown in Figure 1. The tank models show the local stress concentrations in the proximity of this openings. Table 2 summarizes the FE cases and subcases developed in this research and provides geometric information of each model.

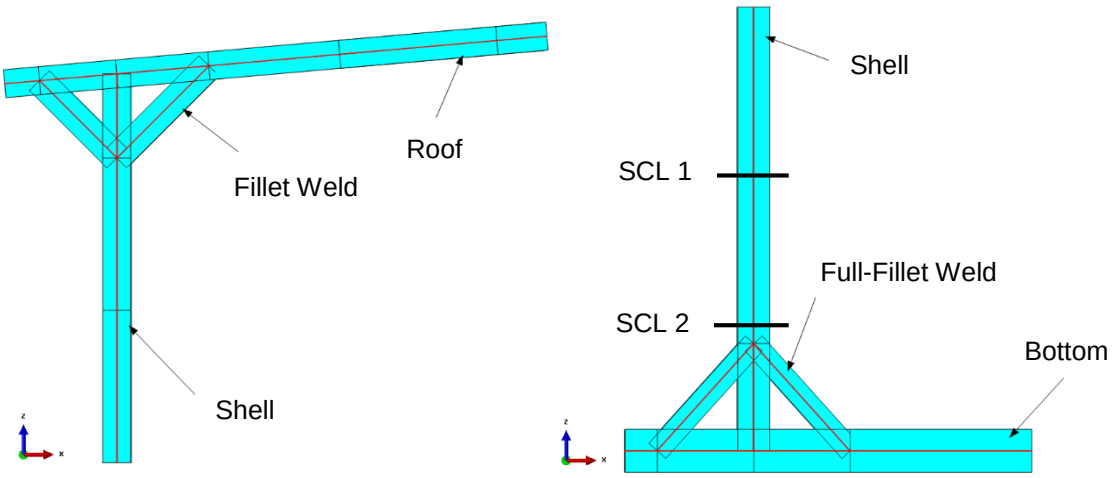

Figure 5. Top and bottom welded joints.

Since the models shall be capable of estimating the bottom uplift at specific pressures, linear elastic springs acting along the vertical Z direction were attached to the tank bottom elements to simulate the soil interaction with the tank. Only compression springs were considered in the analysis. Thus, after applying the liquid and internal pressure as well as

the self-weight, those springs in tension were removed from the models. Furthermore, the analysis considered that the unanchored tanks were placed over a compacted sand soil and supported by concrete ringwalls six inches wide measured from the tank shell. Therefore, the spring stiffness assumed subgrade modulus of 250 lbf/in^3 (68000 kN/m^3) and 1000 lbf/in^3 (270000 kN/m^3) to represent the compacted sand base and the concrete ringwall, respectively [5]. Finally, the mechanical properties of the A36 steel materials as well as additional tank dimensions are presented in Table 3.

The tank models were subjected to internal pressure and hydrostatic pressure with 18 in. (0.45 m) of product level and the tank half full. The density of water was taken as 62.4 lb/ft^3 (1000 kg/m^3). Four types of analyses were carried out to determine the failure modes of the finite element models, i.e. elastic stress analysis, elastic buckling mode analysis, elastic-plastic analysis, and wind load analysis. Considering the different thirteen API 12F tanks as well as all the geometric parameters, a total of 356 finite element models were studied throughout this research.

Table 2. Summary of FE cases and subcases

Cases	Diameter	Height
	ft-in (m)	ft (m)
1	7-11 (2.4)	10 (3.0)
2	9-6 (2.9)	8 (2.4)
3	9-6 (2.9)	12 (3.7)
4	12 (3.7)	10 (3.0)
5	10 (3.0)	15 (4.6)
6	11 (3.4)	15 (4.6)
7	12 (3.7)	15 (4.6)
8	12 (3.7)	20 (6.1)
9	12 (3.7)	25 (7.6)
10*	15-6 (4.7)	16 (4.9)
11*	15-6 (4.7)	24 (7.3)
12*	15-6 (4.7)	30 (9.1)
13*	21-6 (6.6)	16 (4.9)

* These cases included rafters when the roof thickness was 3/16 in.

Sub cases	Shell Thick	Roof Thick	Bottom Thick	Liquid Levels	Internal Pressure
	in (mm)	in (mm)	in (mm)	in (m)	
A	3/16 (4.8)	3/16 (4.8)	1/4 (6.4)	18 (0.45)	Bottom Joint Yielding
B	3/16 (4.8)	3/16 (4.8)	1/4 (6.4)	18 (0.45)	Top Joint Yielding
C	3/16 (4.8)	3/16 (4.8)	1/4 (6.4)	-	Buckling
D	3/16 (4.8)	3/16 (4.8)	1/4 (6.4)	Half Full	Wind Pressure
E	3/16 (4.8)	3/16 (4.8)	3/8 (9.5)	18 (0.45)	Bottom Joint Yielding
F	3/16 (4.8)	3/16 (4.8)	3/8 (9.5)	18 (0.45)	Top Joint Yielding
G	3/16 (4.8)	3/16 (4.8)	3/8 (9.5)	-	Buckling
I	3/16 (4.8)	3/16 (4.8)	1/4 (6.4)	18 (0.45)	Design Pressure
J	3/16 (4.8)	3/16 (4.8)	3/8 (9.5)	18 (0.45)	Design Pressure
K	3/16 (4.8)	3/16 (4.8)	1/4 (6.4)	Half Full	Bottom Joint Yielding
L	3/16 (4.8)	3/16 (4.8)	1/4 (6.4)	Half Full	Top Joint Yielding
M	3/16 (4.8)	3/16 (4.8)	3/8 (9.5)	Half Full	Bottom Joint Yielding
N	3/16 (4.8)	3/16 (4.8)	3/8 (9.5)	Half Full	Top Joint Yielding
O	3/16 (4.8)	3/16 (4.8)	1/4 (6.4)	18 (0.45)	Plastic Collapse
P	3/16 (4.8)	3/16 (4.8)	3/8 (9.5)	18 (0.45)	Plastic Collapse
Q	3/16 (4.8)	3/16 (4.8)	1/4 (6.4)	Half Full	Plastic Collapse
R	3/16 (4.8)	3/16 (4.8)	3/8 (9.5)	Half Full	Plastic Collapse
A2	1/4 (6.4)	1/4 (6.4)	1/4 (6.4)	18 (0.45)	Bottom Joint Yielding
B2	1/4 (6.4)	1/4 (6.4)	1/4 (6.4)	18 (0.45)	Top Joint Yielding
C2	1/4 (6.4)	1/4 (6.4)	1/4 (6.4)	-	Buckling
D2	1/4 (6.4)	1/4 (6.4)	1/4 (6.4)	Half Full	Wind Pressure
E2	1/4 (6.4)	1/4 (6.4)	3/8 (9.5)	18 (0.45)	Bottom Joint Yielding
F2	1/4 (6.4)	1/4 (6.4)	3/8 (9.5)	18 (0.45)	Top Joint Yielding
G2	1/4 (6.4)	1/4 (6.4)	3/8 (9.5)	-	Buckling
I2	1/4 (6.4)	1/4 (6.4)	1/4 (6.4)	18 (0.45)	Design Pressure
J2	1/4 (6.4)	1/4 (6.4)	3/8 (9.5)	18 (0.45)	Design Pressure
K2	1/4 (6.4)	1/4 (6.4)	1/4 (6.4)	Half Full	Bottom Joint Yielding
L2	1/4 (6.4)	1/4 (6.4)	1/4 (6.4)	Half Full	Top Joint Yielding
M2	1/4 (6.4)	1/4 (6.4)	3/8 (9.5)	Half Full	Bottom Joint Yielding
N2	1/4 (6.4)	1/4 (6.4)	3/8 (9.5)	Half Full	Top Joint Yielding
O2	1/4 (6.4)	1/4 (6.4)	1/4 (6.4)	18 (0.45)	Plastic Collapse
P2	1/4 (6.4)	1/4 (6.4)	3/8 (9.5)	18 (0.45)	Plastic Collapse
Q2	1/4 (6.4)	1/4 (6.4)	1/4 (6.4)	Half Full	Plastic Collapse
R2	1/4 (6.4)	1/4 (6.4)	3/8 (9.5)	Half Full	Plastic Collapse

Table 3. Additional tank dimensions.

	Dimensions	
	(US customary)	(SI)
Young's Modulus	2.9×10^7 psi	2.0×10^5 MPa
Poisson's Ratio	0.3	0.3
Steel Density	490 lb/ft^3	7850 kg/m^3
A36 Yield strength	36 ksi	250 MPa
A36 Tensile strength	58 ksi	400 MPa
Roof Slope	1:12	1:12
Rafter's Beam Shape	C6x8.2	C6x8.2
Column Pipe	6 in. STD	150 mm STD
Ring Plate Thick	1/4 in.	6.35 mm
Chime Projection	3/8 in.	9.5 mm
Bottom Joint Weld	Full-fillet	Full-fillet
Top Joint Weld	Max 3/16 in. Fillet	Max 5 mm Fillet
Top clean-out	24 in. wide 36 in. high	610 mm wide 915 mm high
Sand base modulus	250 lbf/in^3	68000 kN/m^3
Ring-wall Modulus	1000 lbf/in^3	270000 kN/m^3
Water Density	62.4 lb/ft^3	1000 kg/m^3

2.3.1 Elastic Stress Analysis

An elastic analysis was developed considering the elastic range of the ASTM A36 steel material of the tank to evaluate the relative strength of the roof-to-shell and bottom- to-shell joints as well as to determine the limiting internal pressure that causes yielding in the tank. Hence, the models were studied to find the internal pressure that produced bottom and roof yielding considering the tanks' dimensions, range of thicknesses, and different liquid product levels and weld sizes.

Moreover, the elastic analysis was carried out to investigate the maximum design pressure of all the thirteen API 12F tank sizes. This research reports the uplift pressure of each tank

as well as the stress levels and vertical displacement values at the shell-to-bottom joint after raising the design pressure to failure or 24 oz./in^2 (10.3 kPa).

Von Mises equivalent stresses were computed at the integration point in the mid-surface of the shell elements of the tanks. This type of stress contemplates the hoop and meridional component stress distributions along with the three principal stress values of each element. The von Mises equivalent stress is calculated using Equation (5).

$$s_e = \sigma_e = \frac{1}{\sqrt{2}}[(\sigma_1 - \sigma_2)^2 + (\sigma_2 - \sigma_3)^2 + (\sigma_3 - \sigma_1)^2]^{0.5} \quad (5)$$

Where s_e or σ_e are the von Mises equivalent stress and σ_1, σ_2, σ_3 are the three principal stresses at the evaluation point in the shell. Additionally, hand calculations were carried out following the API 937 guidelines to determine the failure and uplift pressures and compare them with the results obtained from the FE models.

2.3.2 Elastic Buckling Mode Analysis

An Eigenvalue buckling analysis was used to estimate the critical buckling modes of the tank models. This analysis calculates the load required to convert the stiffness matrix of the problem to singular. The first positive eigenvalue represents the internal pressure that produces the first buckling mode in the tank, this value is reported in this investigation [12]. Negative eigenvalues were neglected because they do not have physical meaning in this investigation. Thus, the Lanczos extraction method was used to optimize the simulation time [13]. Additionally, the membrane equivalent stress was compared to $0.55S_y$ (S_y is yield stress of material) as stated in the API 579 [14] to ensure that the buckling stresses remain in the elastic range.

The purpose of this analysis is to investigate the structural stability of the API 12F steel tanks as well as determine the influence of the critical buckling pressure in the failure mode of the tanks. Hence, complete 3-D tank models were constructed for this analysis and, following the structural analysis of the API 937, a buckling mode with many waves was expected to occur in the models.

2.3.3 Elastic-Plastic Stress Analysis

Even though the API 650 Annex F [7] describes the tank's failure pressure as the one that causes yielding in the compression ring area, plastic collapse of the API 12F tanks was investigated in this research using an elastic-plastic analysis. The stress redistribution and inelastic deformations were considered in the numerical analysis by including an elastic-plastic steel material in the computations. Finite element models were built to show the non-linear deformations due to the internal pressure. Moreover, no imperfections or fabrication tolerances were included in the analysis. The results of these analyses showed the failure pressure that causes structural instability in the tank by producing large deformation for a small increase of load or by the inability of the model to resist more acting pressure achieving the plastic collapse.

An elastic plastic material was used, and plastic hardening was included up to the true ultimate stress in the analysis. ASME BPVC 2013, Section VIII, Division 2 [15] was referenced to obtain the true stress-strain curve used in the computational models. The material was considered isotropic and elastic-plastic with Young's modulus $E = 2.9 \times 10^7$ psi (2.0×10^5 MPa), yield strength $F_y = 36$ ksi (250 MPa) and the ultimate

tensile strength F_u = 58 ksi (400 MPa) corresponding to the ASTM A36 steel material. The true stress-strain curve used in the finite element simulations is shown in Figure 6.

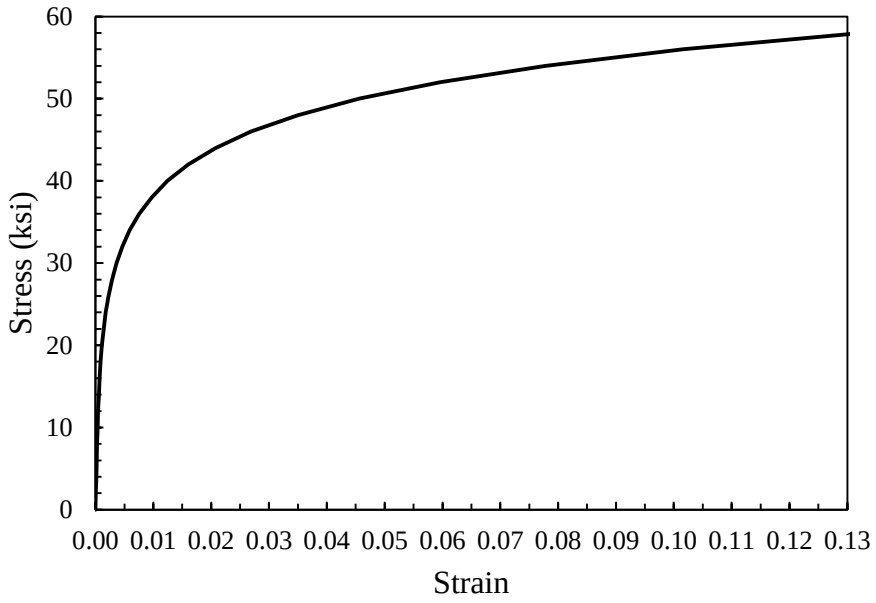

Figure 6. Stress-strain curve of mild steel material

The modified Riks method [16] was used to predict the unstable, geometrically nonlinear collapse of the tank models. In general, this method is used when a structure must release strain energy to remain in equilibrium, and the load value is unknown. Since the purpose of this analysis was to investigate the plastic collapse of the tanks considering significant geometry changes and the material nonlinearity, a load-displacement (Riks) analysis was suitable to accurately evaluate the behavior of the models. The analysis was carried out in two steps. First, the selfweight and liquid pressure were applied to the model. Second, the Riks method was perfomed, an initial unit internal pressure or reference load was applied to the tank and proportionally increased to achieve the plastic collapse pressure. According to the Abaqus User Manual [10], the Riks method treats the load magnitude as an additional unknown and simultaneously solves loads and displacements. However, some nonlinear

models may have convergence problems because of excessive distortions or very large plastic strain increments.

2.3.4 Wind Load Analysis

A wind load was applied to the cylindrical shell and conical roof of the 12 ft. (3.7 m) diameter and 25 ft. (7.6 m) high shop-welded tank. This tank model was selected as a reference for further investigations since it has the greatest height-diameter ratio (H/D = 2.1) among the API 12F tanks. The wind pressure was calculated in accordance with the API 650 standard [7] using a wind speed of 90 mph (145 km/h), and the ASTM A36 steel material was considered to remain elastic. Moreover, the tank was assumed to be half full of product with specific gravity (SG). of 0.7 based on API 650 paragraph 5.11.2.3 [7].

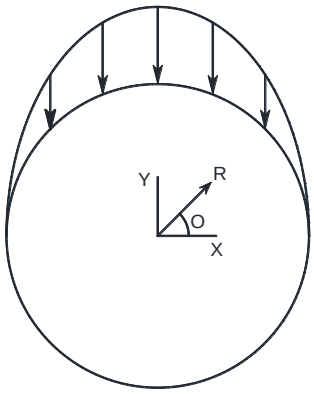

Figure 7. Wind pressure distribution over the shell

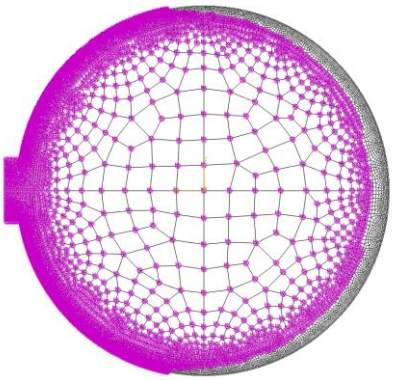

Figure 8. Springs distribution on the tank bottom

The internal pressures for 3/16 in. (4.8 mm) and 1/4 in. (6.4 mm) thick shells and roofs were 5.5 oz./in^2 (2.4 kPa) and 7.0 oz./in^2 (3.0 kPa), respectively. Since ABAQUS does not provide a projected area loading option, a sinusoidal function was approximated to apply

the horizontal wind pressure to the cylindrical shell as seen in Figure 7 [17]. Also, the wind uplift pressure was uniformly distributed on the conical roof. Finally, several iterations were carried out to remove the linear elastic springs and to only consider the springs in compression during the analysis. A typical distribution of the springs under the tank subjected to some uplift is shown in Figure 8.

2.4 Analysis and Discussion

The present study evaluated the failure pressure of the current eleven and two proposed API 12F shop welded, flat bottom, tanks. The shell and roof thicknesses, the bottom thickness as well as the product level were evaluated to determine their influence in the failure of the tanks. Moreover, four different analyses were carried out to address the objective of this research. The elastic stress analysis determined the internal pressure that produced yielding in the cross section of the roof-to-shell and shell-to-bottom joints, the elastic buckling mode analysis reported the buckling internal pressure of the tank, the elastic-plastic analysis evaluated the rupture pressure of each API 12F tank and the wind load analysis presented the stresses and uplift of a API 12F due to a wind pressure.

Since several finite element models were studied in this investigation, the thirteen API 12F shop welded tanks were classified in four groups according to their diameters to summarize the results. Table 4 to Table 7 show the internal pressure ranges obtained for each group of tanks.

Table 4. Summary of yielding and buckling pressures for tanks with diameters from 7ft. 11in. (2.4 m) to 11ft (3.4 m).

Tank Diameter 7ft.11in. to 11 ft.		
	Shell Thickness	
	3/16 in	1/4 in
Roof to Shell Yielding Pressure (psi)	5.8-9.5	8.0-13.2
Bottom to Shell Yielding Pressure (psi)		
Bottom Thick. 1/4 in and Product Level: 18 in	6.5-10.5	8.3-13.4
Bottom Thick. 3/8 in and Product Level: 18 in	7.1-11.5	10.5-16.9
Bottom Thick. 1/4 in and Product Level: Half Full	7.4-11.0	9.4-14.10
Bottom Thick. 3/8 in and Product Level: Half Full	8.0-12.0	11.5-17.6
Buckling Pressure (psi)		
Bottom Thick. 1/4 in	7.3-18.8	16.4-43.1
Bottom Thick. 3/8 in	7.3-18.8	16.4-43.1

Table 5. Summary of yielding and buckling pressures for tanks with 12 ft. (3.7 m) diameter

Tank Diameter 12ft.		
	Shell Thickness	
	3/16 in	1/4 in
Roof to Shell Yielding Pressure (psi)	4.9	6.8
Bottom to Shell Yielding Pressure (psi)		
Bottom Thick. 1/4 in and Product Level: 18 in	5.6-5.9	7.1-7.6
Bottom Thick. 3/8 in and Product Level: 18 in	6.2-6.5	9.0-9.5
Bottom Thick. 1/4 in and Product Level: Half Full	6.1-7.4	7.7-9.3
Bottom Thick. 3/8 in and Product Level: Half Full	6.7-8.0	9.6-11.1
Buckling Pressure (psi)		
Bottom Thick. 1/4 in	5.0-5.2	11.2-11.7
Bottom Thick. 3/8 in	5.0-5.2	11.2-11.7

Table 6. Summary of yielding and buckling pressures for tanks with 15 ft. 6 in. (4.7 m) diameter

Tank Diameter 15 ft. 6in.		
	Shell Thickness	
	3/16 in	1/4 in
Roof to Shell Yielding Pressure (psi)	4.6	4.6
Bottom to Shell Yielding Pressure (psi)		
Bottom Thick. 1/4 in and Product Level: 18 in	4.0-4.3	5.1-5.5
Bottom Thick. 3/8 in and Product Level: 18 in	4.4-4.9	6.4-7.0
Bottom Thick. 1/4 in and Product Level: Half Full	4.8-5.9	6.0-7.3
Bottom Thick. 3/8 in and Product Level: Half Full	5.2-6.5	7.3-8.8
Buckling Pressure (psi)	(Rafters)	
Bottom Thick. 1/4 in	4.9-5.1	5.4
Bottom Thick. 3/8 in	5.0-5.5	5.4

Table 7. Summary of yielding and buckling pressures for tank with 21 ft. 6 in. (6.6 m) diameter.

Tank Diameter 21ft.6in.		
	Shell Thickness	
	3/16 in	1/4 in
Roof to Shell Yielding Pressure (psi)	2.7	2.8
Bottom to Shell Yielding Pressure (psi)		
Bottom Thick. 1/4 in and Product Level: 18 in	2.6	3.0
Bottom Thick. 3/8 in and Product Level: 18 in	3.0	4.1
Bottom Thick. 1/4 in and Product Level: Half Full	3.3	4
Bottom Thick. 3/8 in and Product Level: Half Full	3.6	4.8
Buckling Pressure (psi)	(Rafters)	
Bottom Thick. 1/4 in	2.1	2.0
Bottom Thick. 3/8 in	2.4	2.0

It was verified that roof-to-shell yielding is not greatly affected by the tank height. Figure 9 and Figure 10 show that tanks with the same diameter (9 ft. 6 in, 12 ft. and 15 ft. 6 in.) and different heights yielded in the top joint at nearly the same internal pressure. Moreover, the roof-to-shell joint failed before the shell-to-bottom joint for most of the tanks. However,

it was found in five models that cross-sectional yielding due to internal pressure occurred first at the bottom juncture. The tanks strength was further analyzed and the relative strength ratio between the shell-to-bottom and roof-to-shell can be observed in Figure 11 and Figure 12. It is important to note that in order to guarantee a frangible roof behavior, the relative strength ratio must be larger than one. Five tank models with shell thickness of 3/16 in. (4.8 mm) reported a ratio smaller than one and the largest value obtained was 1.63. All the models with shell thickness of 1/4 in. (6.4 mm) reported relative strength ratios larger than one. The smallest and largest values were 1.01 and 1.91 respectively.

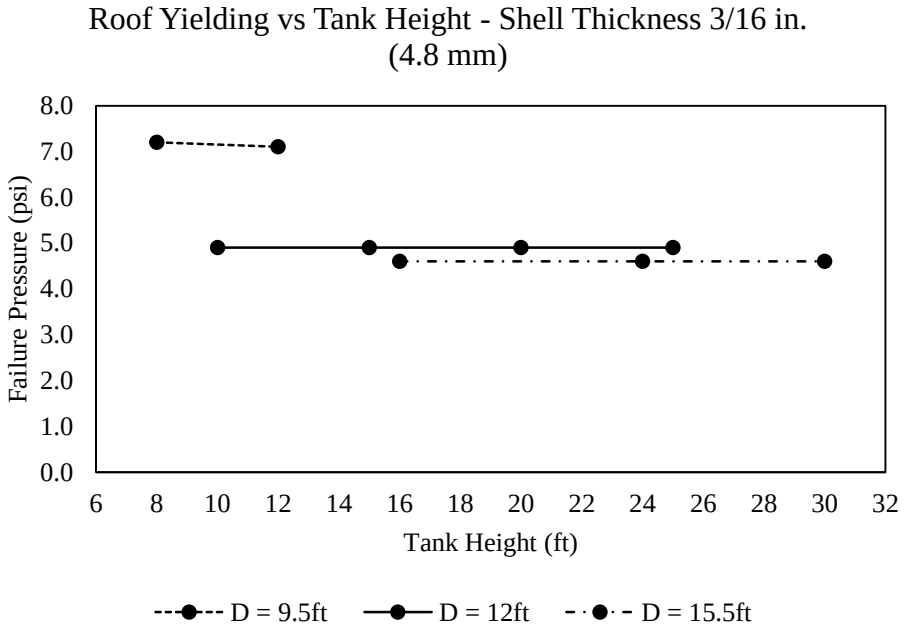

Figure 9. Effect of the tank height in the top joint yielding

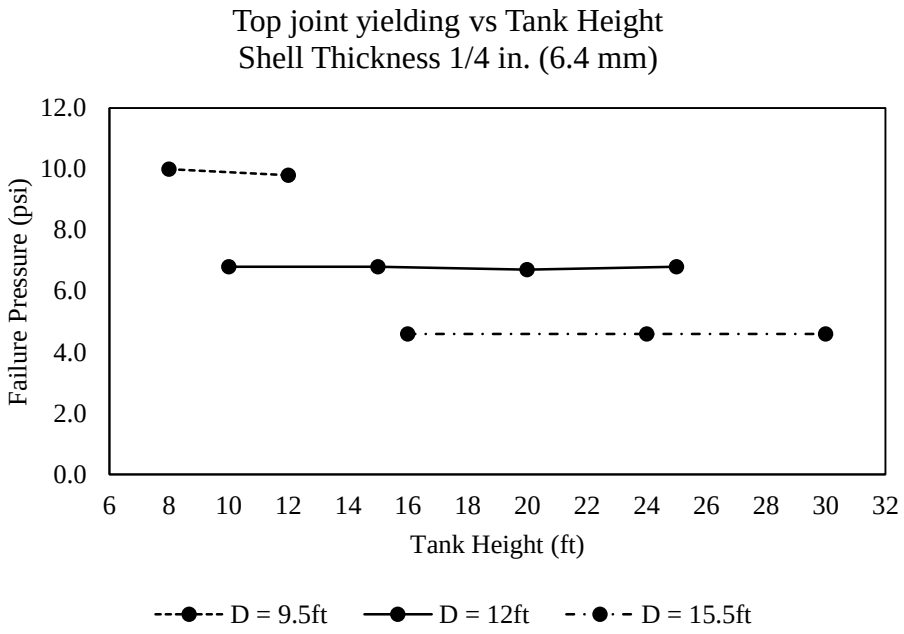

Figure 10. Effect of the tank height in the top joint yielding

Figure 13 and Figure 14 compare the smallest yielding pressure (minimum of roof-to-shell or shell-to-bottom yielding pressures) of the tanks with the API 937 failure pressure obtained through hand calculations using Equation (3). As it was concluded in the API 937, the hand calculations provided significantly lower results than the finite elements analysis. In general, the ratios between FEA computations and API 937 results were equal or greater than 3. Moreover, the uplift pressure results computed by FEA and the API 937 formulation using Equation (2) were included in Figure 13 and Figure 14, both methods reported similar results. It can be noted that the uplift pressures are considerably smaller than the critical yielding pressures for all the tank models studied. Even though the tanks experienced some uplift before yielding at the top joint, failure at the bottom joint was far from occurring.

The maximum design pressure of all the thirteen tank models was investigated in this study. In all the cases examined, the 24 oz/in^2 (10.3 kPa) pressure did not cause failure

of the roof-to-shell or shell-to-bottom joints. However, relevant uplift was observed especially in bigger diameter tanks as a result of applying such pressure. Table 8 and Table 9 report the uplift values obtained through FEA as well as the membrane and membrane plus bending equivalent stresses occurring through two stress classification lines (SCL) at the shell-to-bottom joint as consequence of the applied pressure and the tank deformations. The two SCL show the highest membrane and highest membrane plus bending stresses at the bottom joint of the tank. The locations of SCL are shown in Figure 5.

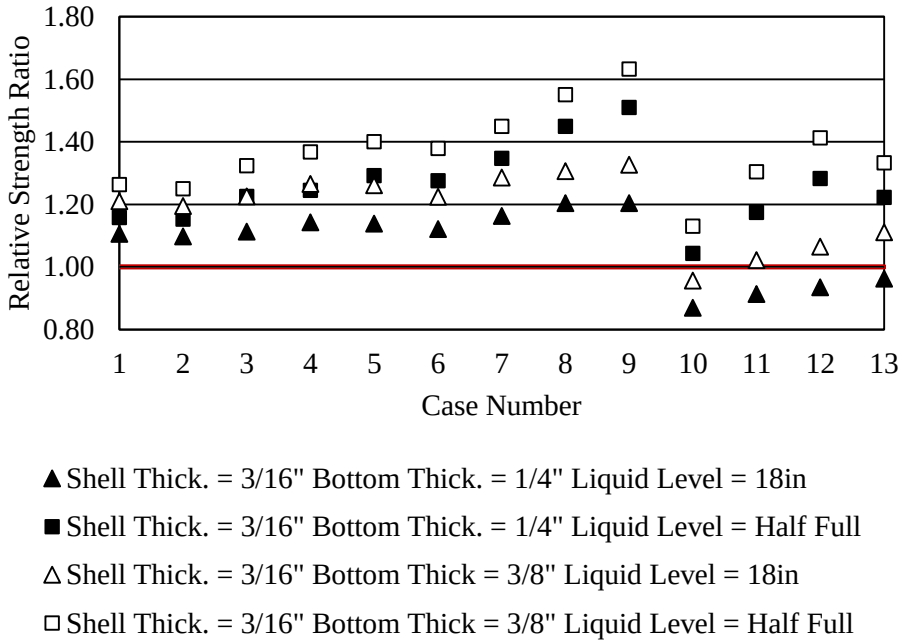

Figure 11. Relative Strength Ratio (shell-to-bottom strength / roof-to-shell strength) for tanks with 3/16 in. (4.8 mm) shell thickness

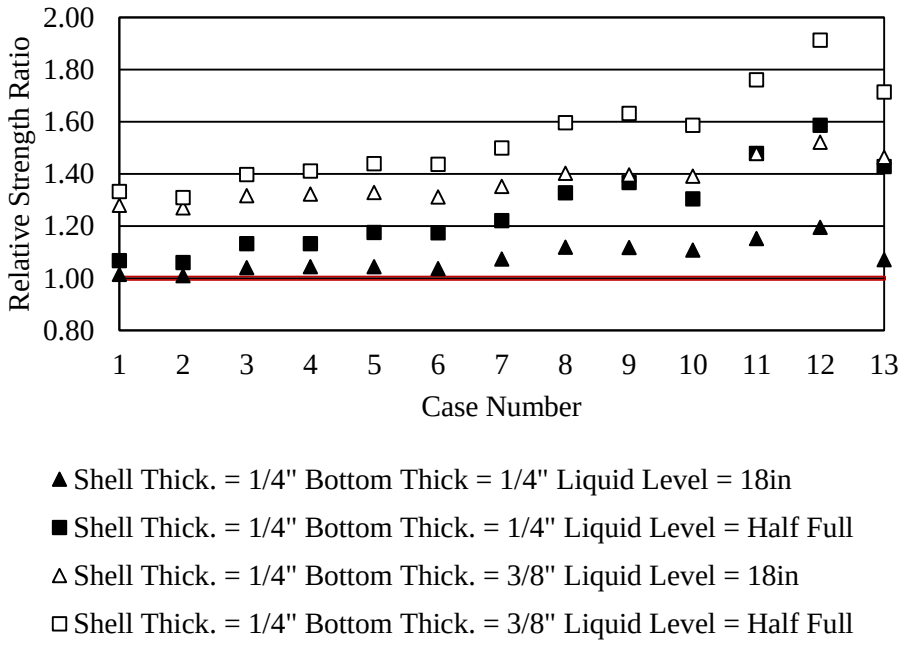

Figure 12. Relative Strength Ratio (shell-to-bottom strength / roof-to-shell strength) for tanks with 1/4 in. (6.4 mm) shell thickness

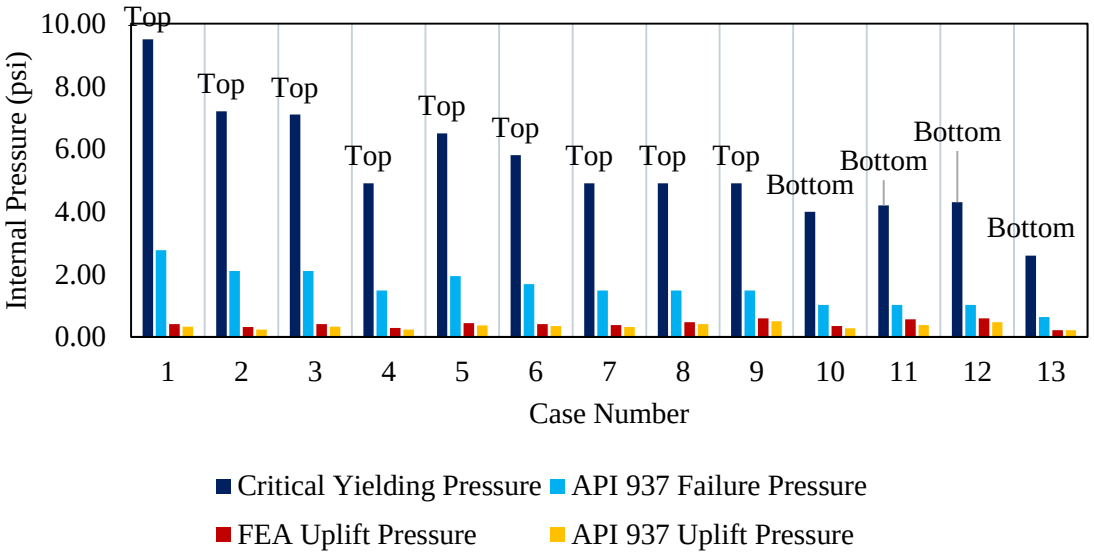

Figure 13. Critical Yielding Pressure occurring at the top or bottom joints, uplift pressure obtained through FEA, and failure and uplift pressures computed by hand calculations using API 937 formulation. Tanks with 3/16 in. (4.8 mm) shell thickness

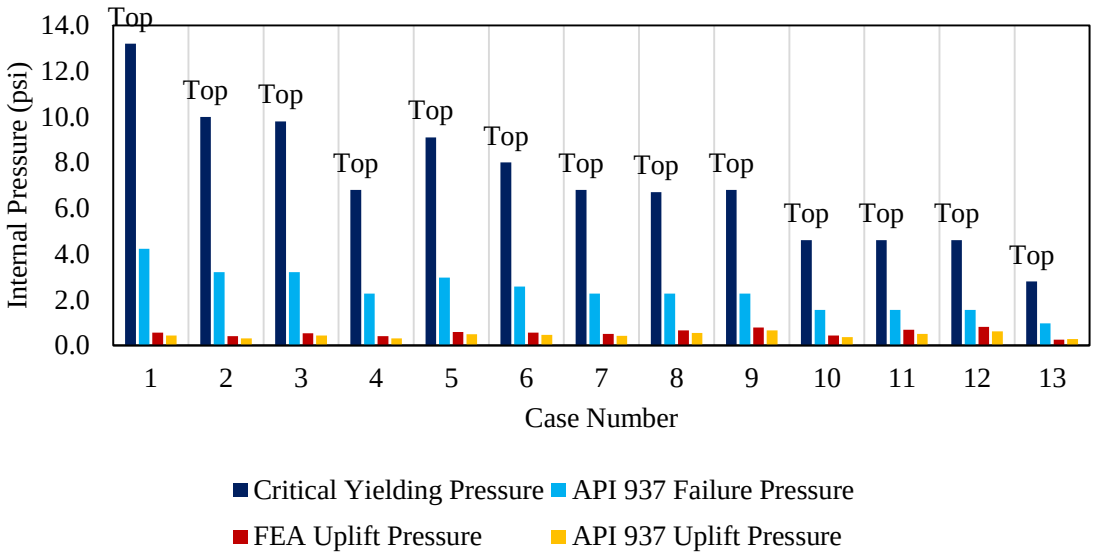

Figure 14. Critical Yielding Pressure occurring at the top or bottom joints, uplift pressure obtained through FEA, and failure and uplift pressures computed by hand calculations using API 937 formulation. Tanks with 1/4 in. (6.4 mm) shell thickness

Table 8. Uplift and stresses occurring at the shell-to-bottom joint due to a 24 oz/in² (10.3 kPa) pressure - Shell thickness 3/16 in (4.8 mm). SCL1: Highest membrane stress at bottom joint. SCL2: Highest membrane plus bending stress at bottom joint

Case	Diameter	Height	Shell Thick.	Bottom Thick.	Stress Classification Line 1		Stress Classification Line 2		Bottom Uplift
					Memb	Memb + Bend	Memb	Memb + Bend	
	ft, in (m)	ft (m)	in (mm)	in (mm)	(psi)	(psi)	(psi)	(psi)	(in)
1	7, 11 (2.4)	10 (3.0)	3/16 (4.8)	1/4 (6.4)	4242	8999	3368	15556	0.3
				3/8 (9.5)	3440	7842	2534	13443	0.16
2	9, 6 (2.9)	8 (2.4)	3/16 (4.8)	1/4 (6.4)	6724	14238	5557	23452	0.59
				3/8 (9.5)	5813	13817	4261	22334	0.37
3	9, 6 (2.9)	12 (3.7)	3/16 (4.8)	1/4 (6.4)	5883	12553	4776	21001	0.48
				3/8 (9.5)	4950	11681	3611	19247	0.29
4	12, 0 (3.7)	10 (3.0)	3/16 (4.8)	1/4 (6.4)	9621	20654	8223	32266	0.92
				3/8 (9.5)	8791	21849	6562	33373	0.69
5	10, 0 (3.0)	15 (4.6)	3/16 (4.8)	1/4 (6.4)	5887	13155	4704	21316	0.48
				3/8 (9.5)	4925	12206	3540	19499	0.28
6	11, 0 (3.4)	15 (4.6)	3/16 (4.8)	1/4 (6.4)	7261	16202	5926	25699	0.65
				3/8 (9.5)	6260	15797	4518	24605	0.42
7	12, 0 (3.7)	15 (4.6)	3/16 (4.8)	1/4 (6.4)	8617	19140	7181	29586	0.81
				3/8 (9.5)	7701	19560	5600	29828	0.57
8	12, 0 (3.7)	20 (6.1)	3/16 (4.8)	1/4 (6.4)	7574	13594	6128	27110	0.69
				3/8 (9.5)	6556	13363	4643	25977	0.45
9	12, 0 (3.7)	25 (7.6)	3/16 (4.8)	1/4 (6.4)	6508	12102	5130	24078	0.55
				3/8 (9.5)	5456	11332	3804	22097	0.34
10	15, 6 (4.7)	16 (4.9)	3/16 (4.8)	1/4 (6.4)	12445	29447	10622	42279	1.28
				3/8 (9.5)	11656	25908	8437	44740	1.03
11	15, 6 (4.7)	24 (7.3)	3/16 (4.8)	1/4 (6.4)	9598	25197	8108	37034	1.05
				3/8 (9.5)	8591	21049	6154	37920	0.76
12	15, 6 (4.7)	30 (9.1)	3/16 (4.8)	1/4 (6.4)	7426	21810	6225	32836	0.84
				3/8 (9.5)	6164	16914	4453	32044	0.57
13	21, 6 (6.6)	16 (4.9)	3/16 (4.8)	1/4 (6.4)	19087	43735	17105	60666	2.22
				3/8 (9.5)	18156	41017	14075	66416	1.91

Table 9. Uplift and stresses occurring at the shell-to-bottom joint due to a 24 oz/in² (10 kPa) pressure - Shell thickness 1/4 in (6.4 mm). SCL1: Highest membrane stress at bottom joint. SCL2: Highest membrane plus bending stress at bottom joint

Case	Diameter	Height	Shell Thick.	Bottom Thick.	Stress Classification Line 1		Stress Classification Line 2		Bottom Uplift
					Memb	Memb + Bend	Memb	Memb + Bend	
	ft, in (m)	ft (m)	in (mm)	in (mm)	(psi)	(psi)	(psi)	(psi)	(in)
1	7, 11 (2.4)	10 (3.0)	1/4 (6.4)	1/4 (6.4)	2036	5183	1491	8229	0.18
				3/8 (9.5)	1737	3634	1177	7496	0.08
2	9, 6 (2.9)	8 (2.4)	1/4 (6.4)	1/4 (6.4)	3710	8903	1406	16618	0.44
				3/8 (9.5)	3226	7067	2128	13331	0.23
3	9, 6 (2.9)	12 (3.7)	1/4 (6.4)	1/4 (6.4)	2931	7377	813	13368	0.31
				3/8 (9.5)	2523	5510	1656	10713	0.15
4	12, 0 (3.7)	10 (3.0)	1/4 (6.4)	1/4 (6.4)	5719	13180	3205	23517	0.75
				3/8 (9.5)	5125	11846	3450	20648	0.47
5	10, 0 (3.0)	15 (4.6)	1/4 (6.4)	1/4 (6.4)	2790	5861	723	13150	0.28
				3/8 (9.5)	2401	5561	1537	10388	0.14
6	11, 0 (3.4)	15 (4.6)	1/4 (6.4)	1/4 (6.4)	3687	7624	1311	16979	0.43
				3/8 (9.5)	3190	7562	2027	13589	0.22
7	12, 0 (3.7)	15 (4.6)	1/4 (6.4)	1/4 (6.4)	4651	11625	2128	20353	0.59
				3/8 (9.5)	4075	9801	2619	17064	0.33
8	12, 0 (3.7)	20 (6.1)	1/4 (6.4)	1/4 (6.4)	3628	7937	1200	16777	0.42
				3/8 (9.5)	3110	7762	1924	13561	0.22
9	12, 0 (3.7)	25 (7.6)	1/4 (6.4)	1/4 (6.4)	2680	6309	601	13043	0.26
				3/8 (9.5)	2263	5830	1385	10297	0.13
10	15, 6 (4.7)	16 (4.9)	1/4 (6.4)	1/4 (6.4)	8450	18805	5323	29642	1.07
				3/8 (9.5)	7259	15295	4878	29253	0.78
11	15, 6 (4.7)	24 (7.3)	1/4 (6.4)	1/4 (6.4)	6038	15111	3063	23867	0.8
				3/8 (9.5)	4473	13503	2903	22303	0.47
12	15, 6 (4.7)	30 (9.1)	1/4 (6.4)	1/4 (6.4)	4349	12059	1577	20231	0.55
				3/8 (9.5)	3029	8376	1719	17040	0.28
13	21, 6 (6.6)	16 (4.9)	1/4 (6.4)	1/4 (6.4)	15855	30300	11935	47527	2.15
				3/8 (9.5)	13373	32493	10356	48947	1.77

The elastic buckling mode analysis was used to investigate the buckling of the tank models. Figure 15 relates the minimum buckling pressure with the roof-to-shell yielding pressure of the tanks with 3/16 in. (4.8 mm) shell thickness and 1/4 in. (6.4 mm) bottom thickness

as well as the tanks with 1/4 in. (6.4 mm) shell thickness and 1/4 in. (6.4mm) bottom thickness. It can be observed that almost all the tank models reached the top joint yielding before the first buckling mode occurred. Nevertheless, two models (Diameter = 21 ft. 6 in. (6.6m)) presented smaller buckling pressure than roof-to-shell yielding pressure. Figure 16 show typical buckling modes of the roof-to-shell and shell-to-bottom joints. In general, buckling at the top joint happened prior to bottom joint buckling except for the models provided with structural supports in the form of rafters in which the bottom joint buckled before the top joint.

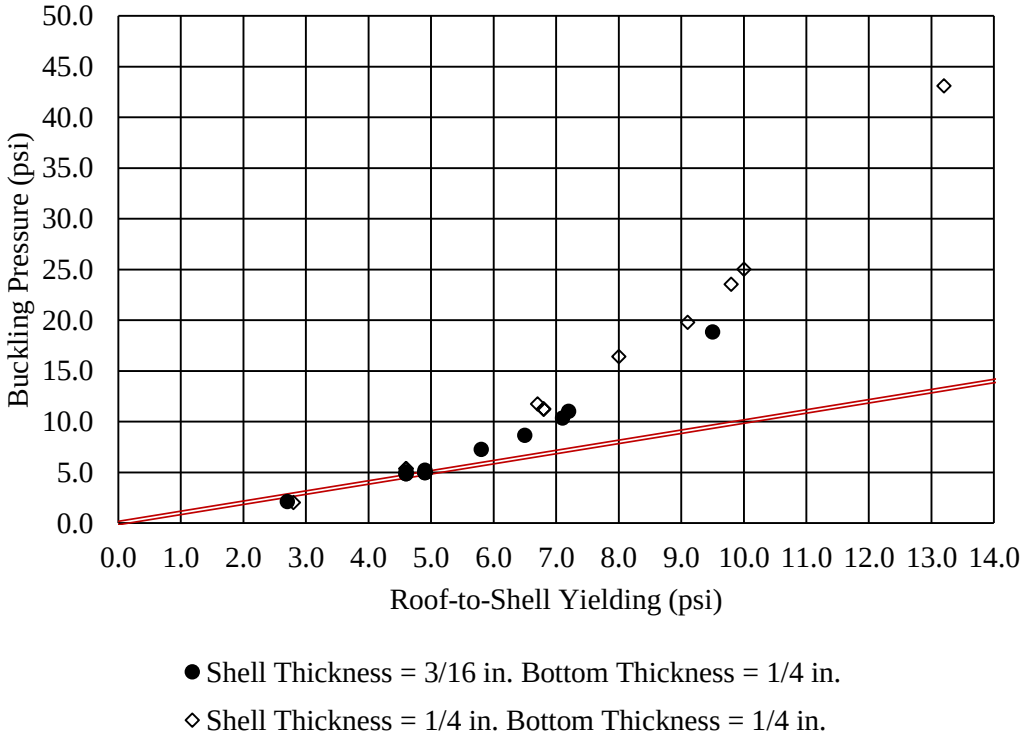

Figure 15. Buckling pressure vs roof-to-shell yielding pressure

Non-linear deformations and plastic collapse of tanks models were investigated using an elastic-plastic stress analysis and the modified Riks method. A typical tank model subjected to internal pressure until rupture is shown in Figure 17. It can be observed the stress levels at all regions of the tank as well as deformations at the top and bottom joints.

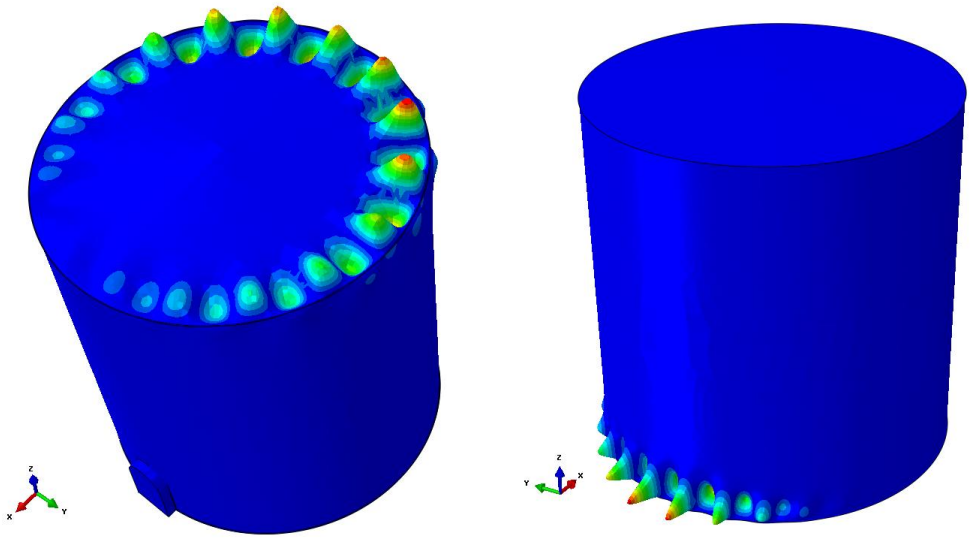

Figure 16. Typical roof-to-shell joint and shell-to-bottom joint buckling modes

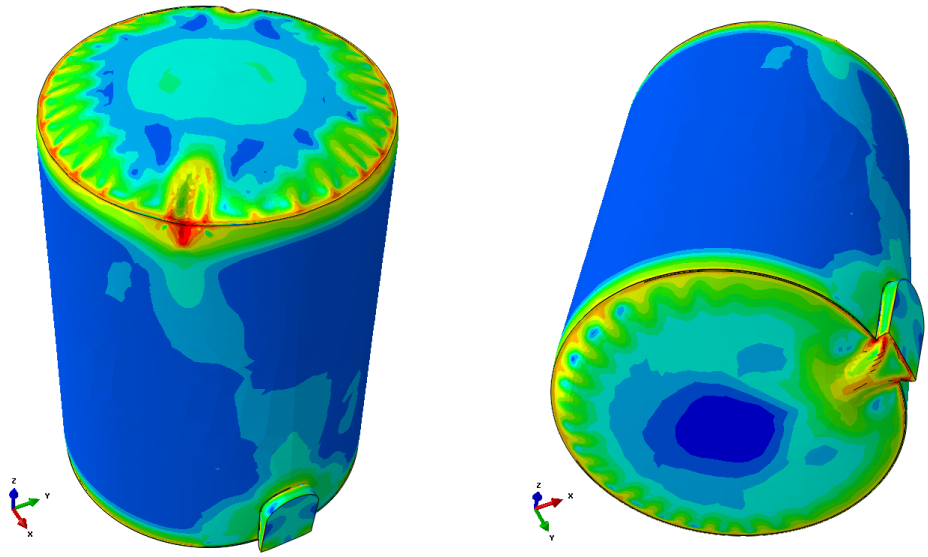

Figure 17. Typical tank model subjected to internal pressure until rupture or plastic collapse

Generally, it was observed that the rupture of the tank occurred in the top joint after applying an excessive internal pressure. Thus, the bottom thickness and product level parameters did not have great impact in the rupture internal pressure. Figure 18 shows a pressure-strain curve for a tank element in rupture. Additionally, the finite element analyses verified that some buckling happened prior the failure of the tank in the roof-to-shell joint. The plastic collapse was compared to the yielding failure and a rupture-to-yielding ratio was computed to evaluate the ductility of the tank models. Hence, it can be observed in Figure 19 and Figure 20 that the rupture-to-yielding ratio ranged from 1.4 to 6.4 and the ductile behavior increased as the tank diameter was smaller.

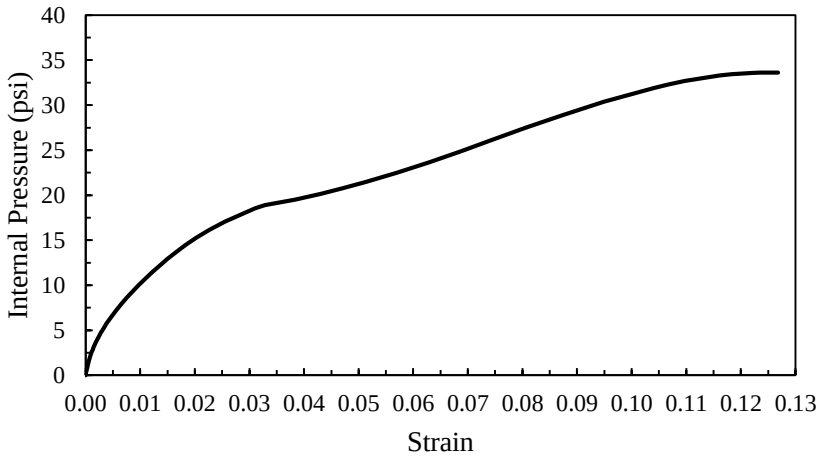

Figure 18. Typical Internal Pressure-Strain Curve

The elastic-plastic analysis was used to study the stress distribution in the proximity of the proposed rectangular and semicircular top clean outs. Even though, the suggested semicircular design is effective to eliminate localized stresses occurring in the shell above the clean out, some stress concentrations were found in the sharp-corners between the clean out neck and the tank bottom. Figure 21 shows typical stress levels of a tank in the vicinity

of the clean out. It is important to note that in all the cases examined, rupture in these sharp-corners occurred before the top or bottom joints failed.

Regarding the wind load analysis developed for the 12 ft. (3.7 m) diameter and 25 ft. (7.6 m) high shop welded tank, Figure 22 shows a scaled deformation as well as the stress levels in the regions of the tank. The analysis results demonstrated that the tank subjected to a 90 mph (145 km/h) wind pressure just experienced small deformations in the form of uplift at the bottom of the tank and low stress distributions mainly in the top and bottom joints. The results are presented in Table 10.

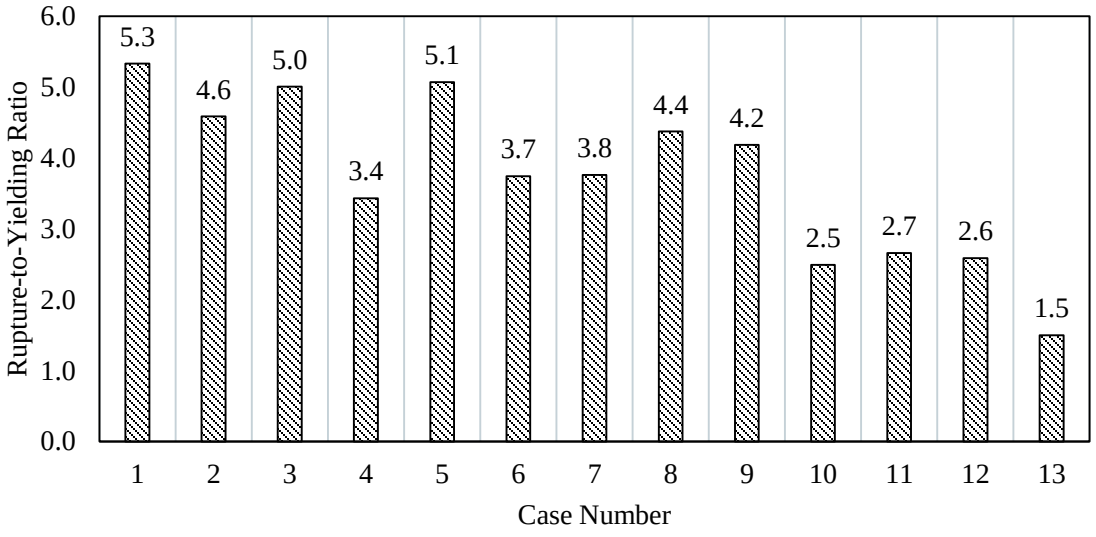

Figure 19. Average rupture-to-yielding ratios for tanks with 3/16 in. (4.8 mm) shell thickness.

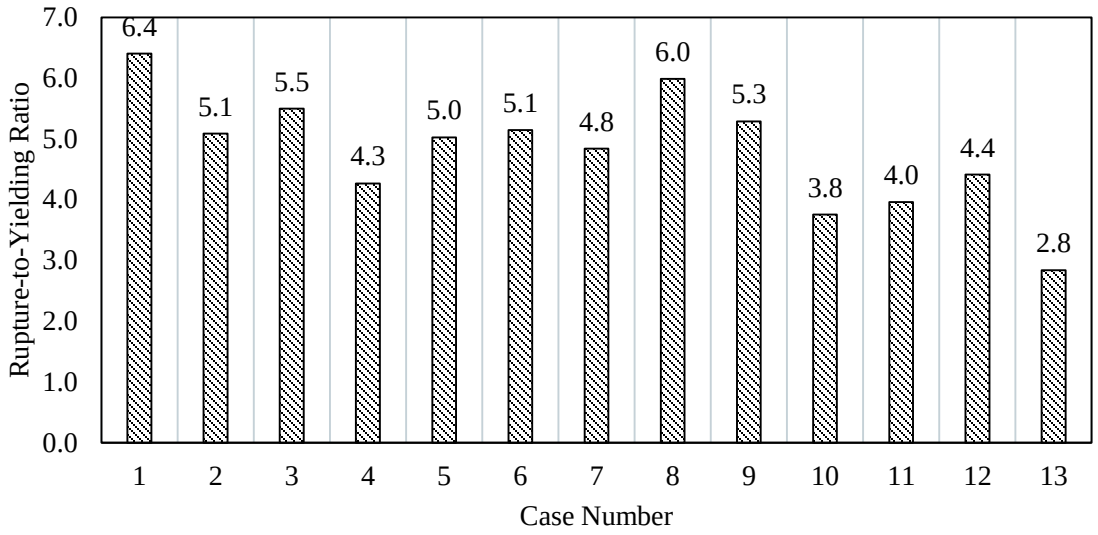

Figure 20. Average rupture-to-yielding ratios for tanks with 1/4 in. (6.4 mm) shell thickness.

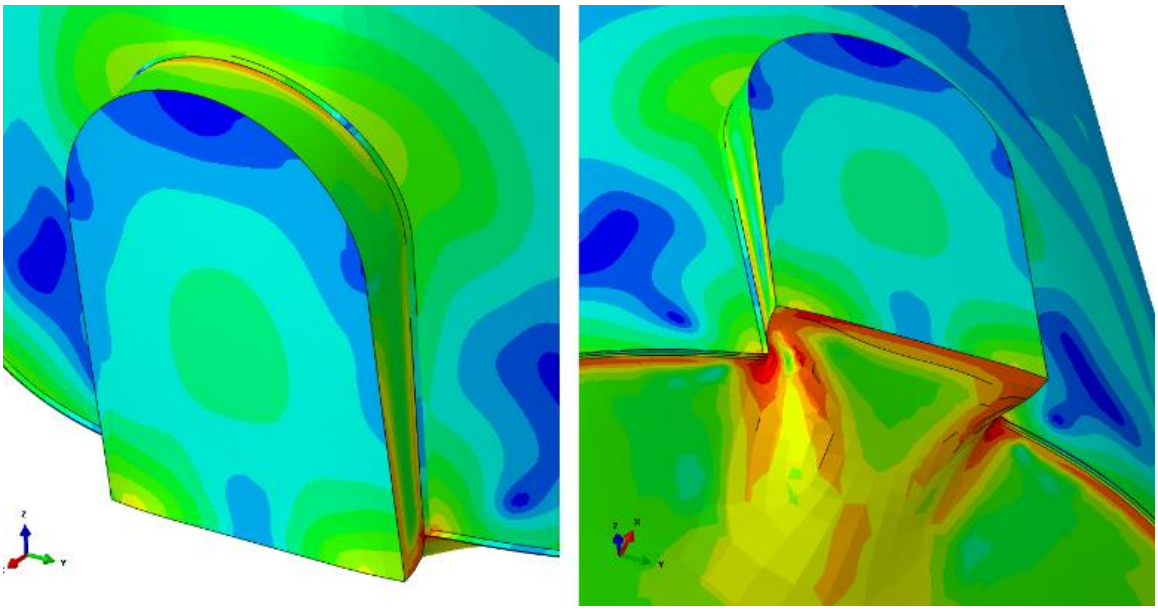

Figure 21. Stress levels of a tank in the vicinity of the clean out.

Table 10. Results of the wind load analysis for the of the 12 ft. (3.7 m) diameter and 25 ft. (7.6 m) high shop-welded tank

Roof-to-Shell Joint Stress	4100 psi
Shell-to-Bottom Joint Stress	1545 psi
Bottom Uplift	0.04 in

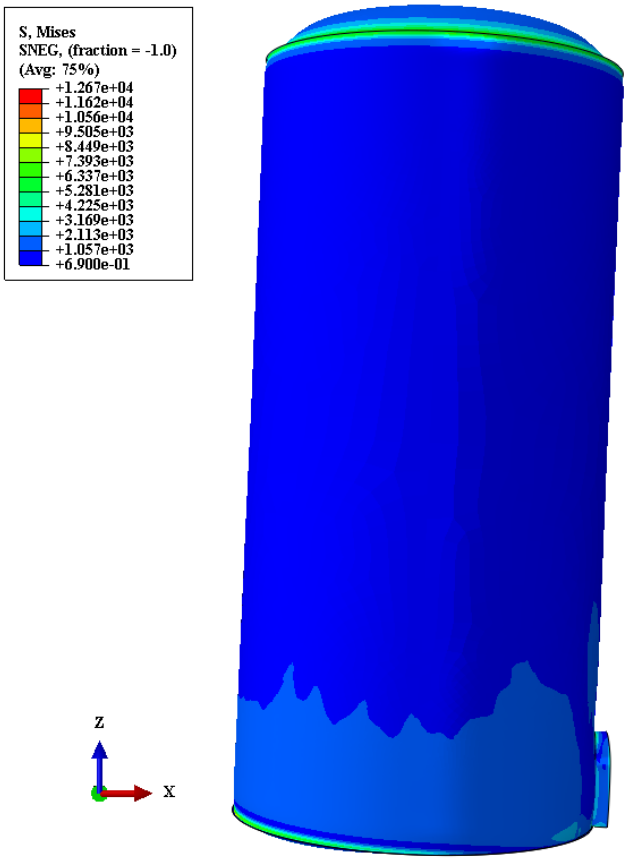

Figure 22. Scaled deformation and stress levels due to wind pressure. (Stresses in psi)

2.5 Conclusions

The present investigation explores the failure pressure modes as well as the maximum design pressure of the API 12F shop-welded, flat bottom tanks for oilfield production liquids through the development of four different analyses: an elastic stress analysis, an elastic buckling mode analysis, an elastic-plastic analysis, and a wind load analysis. This study yields the following conclusions:

- The shell-to-bottom joint strength was evaluated relative to the roof-to-shell joint for the thirteen (13) API 12F tanks considering different shell, roof and bottom thicknesses as well as two product levels, 18 inches and the tank half full. In general, the relative strength ratio was greater than one guaranteeing the frangible roof joint behavior. Nevertheless, five tank models yielded at the bottom joint before failure occurred at the top joint and the relative strength ratio range among all the studied models was between 0.87 and 1.91.
- It was verified in this study that the roof-to-shell joint yielding is not greatly affected by the change of height of the API 12F shop-welded tanks.
- The failure pressure obtained using finite element analyses of the tanks was significantly higher than the calculated according to the API 937 formulation. The ratio of the computations obtained through the two procedures was i equal or greater than 3.
- The API 937 formulation and the finite element analysis are in good agreement regarding the estimation of the bottom uplift of the tanks. Additionally, the results of this study indicated that the API 650 uplift criteria might be too conservative to the API 12F shop-welded tanks. Even though the tank models experienced some

uplift at the bottom, they were capable of resisting further internal pressure before yielding at the top or bottom joints.

- This research investigated the raising of the design pressure of all the thirteen API 12F tanks. It was observed that a pressure of 24 oz/in^2 (10.3 kPa) did not cause yielding at the roof-to-shell or shell-to-bottom joint of any tank. However, significant uplift was observed after applying this internal pressure, especially for tanks with bigger diameters.
- The elastic buckling mode analysis performed in this study indicated that in general buckling occurs after yielding of the tank top joint. Only the 21ft. 6in (6.6 m) diameter tank reported a buckling pressure smaller than the roof-to-shell yielding pressure.
- It was verified that buckling at roof-to-shell joint occurs before the shell-to-bottom joint buckles. Additionally, it was observed that the rafters increase the stiffness of the roof-to-shell joint since the first buckling mode of tank models provided with these structural supports occurred at the bottom joint.
- In general, tanks rupture and ultimate tensile stress was observed at the top joint. Thus, the bottom thickness and product level did not have an important contribution in the range of the results.
- This investigation examined the ductile behavior of the API 12F shop-welded tanks. The rupture-to-yielding ratios among the models ranged from 1.4 to 6.4, being the tanks with smaller diameters more ductile than those with bigger diameters.
- The proposed rectangular and semicircular top clean out design is effective to avoid stress concentrations in the shell above the neck of the attachment. However, some

localized stresses were identified in the sharp corner between the neck and the bottom of the tank. Rupture in the proximity of this opening occurred prior failure of the roof-to-shell joint. It is recommended to perform a fatigue and fracture analysis to estimate the life of the equipment and determine whether or not the sharp-corner detail shall be modified to avoid failure in the base of the tanks.

- The wind load analysis developed in this study indicated that the tank examined (12 ft. (3.7 m) diameter, 25 ft. (7.6 m) high) showed low stress levels in the top and bottom joints and small uplift values at the bottom of the tank. Therefore, the wind pressure was not critical in the analysis of the tank failure modes.
- Even though a vacuum pressure analysis was not within the scope of this study, it is recommended to perform such analysis and compare the failure pressures with the results presented in this report to determine the critical failure modes of the API 12F shop-welded tanks.

CHAPTER 3. FATIGUE ANALYSIS OF THE API 12F TANKS

3.1 Introduction

The specification for shop welded tanks for storage of production liquids, API 12F 0, aims to provide tanks with standard dimensions and capacities to the oil and gas industry. The API 12F sets a tank's dimensions table to be utilized by purchasers and manufactures to identify the nominal capacity and design pressure of specific steel storage tanks required in the field. Particularly, these equipment are fabricated in compliance to design codes and standards such as the API 650 [7] and furnished by the manufacturer for the inspection of the purchaser.

Recently, the American Petroleum Institute (API) has identified the need to study the different failure modes of the API 12F shop welded tanks. The first phase of this project is presented in Chapter 2. The investigation performed an elastic stress analysis to determine the yielding pressure of the tanks. Also, this phase analyzed the buckling modes due to internal pressure in the tanks as well as the plastic collapse of the roof-to-shell and shell-to-bottom joints using an elastic-plastic analysis and considering the plastic hardening of the material and non-linear deformations. The purpose of the present research is further investigate the API 12F flat bottom tanks and determine the fatigue life of these equipment. The ASME BPVC Section VIII, Division 2, 2013 Edition, Part 5 [15] design-by-analysis

requirements were implemented along with finite elements analyses carried out using the software ABAQUS version 6.13 [10].

A fatigue analysis is performed in aboveground storage tanks to estimate the number of pressure cycles caused by different loading conditions that these equipment can resist throughout their operating life. Numerous studies have investigated the fatigue assessment on steel storage tanks [20]-[21], others have focused their research in tank behavior due bottom uplift [22]-[24]. However, to the best of the author's knowledge, no other investigations have addressed the determination of the design fatigue life of the API 12F shop welded tanks subjected to cycles of design internal pressure and vacuum.

Repeated cycles during the operation of the equipment can produce fatigue fractures on the material or welds, leading to environmental threats and important cost impacts to the owner due to spillage of tank contents [2]-[3]. Therefore, engineering designs and calculations must be in compliance with specifications and industry codes to mitigate undesirable failure risks and ensure safety on the equipment operation. The following section provides background information regarding the specifications and codes utilized for the development of the present study.

3.2 Background Information

3.2.1 API 12F Specification for Shop Welded Tanks for Storage of Production Liquids 0

As mentioned before, this API specification provides a group of standard tanks with specific sizes and capacities for the convenience of manufacturers and purchasers. The design of these equipment was developed to offer safe and economic shop-welded tanks to

the petroleum industry for the storage of liquids during the upstream, exploration, and production segment of projects.

Eleven shop-fabricated, flat bottom steel tanks are recommended in this specification. Moreover, two new proposed sizes are in evaluation to be included in the mentioned group. These equipment are fabricated and furnished by a manufacturer according to the need of the client. Besides the tank size and nominal capacity, the purchaser must specify the shell and bottom thicknesses which ensure the structural stability of the equipment during the operation. The tank bottom shall be flat or conical, the roof deck shall be self-supported, cone-type, with a slope of 1 in. (25.4 mm) in 1 ft. (0.3 m). Tanks diameters vary from 7 ft. 11 in. (2.4 m) to 15 ft. 6 in (4.7 m). The tank heights range from 8 ft. (4.7 m) to 24 ft. (7.3 m). Finally, the nominal working capacity of the tanks range from 72 bbl. (11.4 m^3) to 746 bbl. (118.6 m^3).

The thicknesses permitted in the API 12F are 3/16 in. (4.8 mm) or 1/4 in (6.4 mm) for shell and roof , while 1/4 in. (6.4 mm) or 3/8 in. (9.5 mm) for the tank bottom. Tanks with 15 ft. 6 in. (4.7 m) or larger diameter and 3/16 in. (4.8 mm) shell thickness shall be provided with structural supports in the form of rafters at the roof deck. Even though the manufacturer and the purchaser agree to use higher strength materials than the stipulated in the API 12F specification, the minimum thicknesses permitted for the equipment shall not be reduced. A typical API 12F shop welded tank modeled using ABAQUS can be observed in Figure 23.

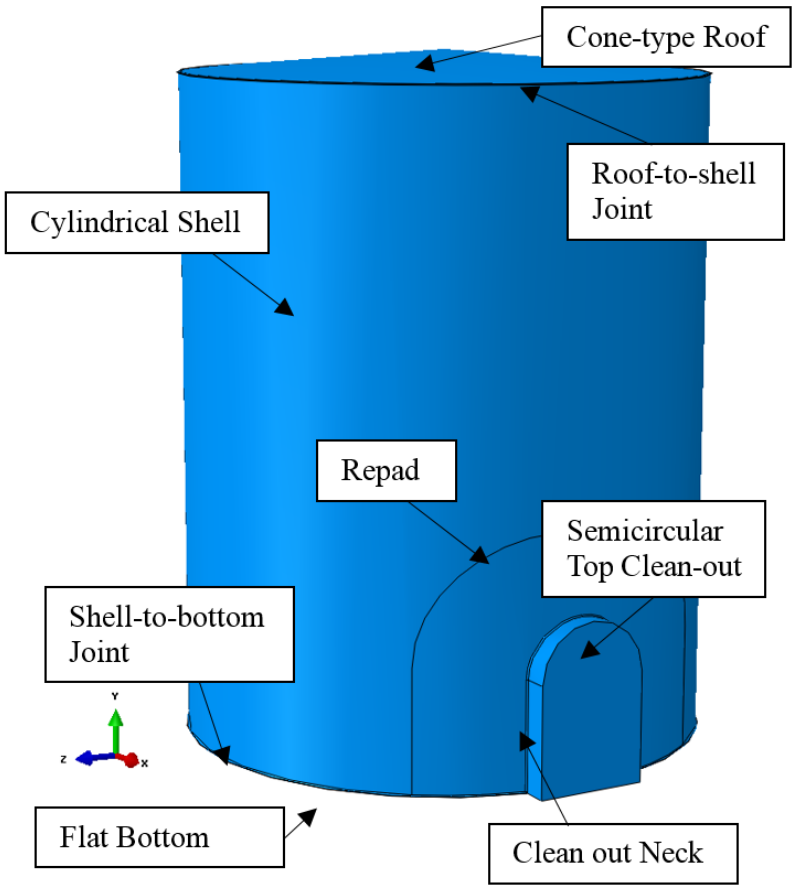

Figure 23. Typical shop-welded, flat-bottom, storage tank with proposed semicircular top clean-out

Table 11 is provided in the API 12F specification to determine the standard tank sizes and maximum design and vacuum operating pressures to ensure safety and stability of the equipment. As mentioned before, two new tank sizes have been proposed to be included in the list, their dimensions are: 21 ft. 6 in. (6.6 m) diameter by 16 ft. (4.9 m) high and 15 ft. 6 in. (4.7 m) diameter by 30 ft. (9.1 m) high.

Table 11. Tank Dimensions

Nominal Capacity	**Design Pressure** oz./in² (kPa)	**Approximate Working Capacity**	**Outside Diameter**	**Height**
bbl, m^3	**Pressure, Vacuum**	bbl, m^3	ft-in. (m)	ft, m
90, 14.3	16, ½ (6.9, 0.2)	72, 11.4	7-11 (2.4)	10, 3.0
100, 15.9	16, ½ (6.9, 0.2)	79, 12.6	9-6 (2.9)	8, 2.4
150, 23.8	16, ½ (6.9, 0.2)	129, 20.5	9-6 (2.9)	12, 3.7
200, 31.8	16, ½ (6.9, 0.2)	166, 26.4	12 (3.7)	10, 3.0
210, 33.4	16, ½ (6.9, 0.2)	200, 31.8	10 (3.0)	15, 4.6
250, 39.7	16, ½ (6.9, 0.2)	224,35.6	11 (3.4)	15, 4.6
300, 47.7	16, ½ (6.9, 0.2)	266, 42.3	12 (3.7)	15, 4.6
400, 63.6	16, ½ (6.9, 0.2)	366, 58.2	12 (3.7)	20, 6.1
500, 79.5	16, ½ (6.9, 0.2)	466, 74.1	12 (3.7)	25, 7.6
500,79.5	8, ½ (3.5, 0.2)	479, 76.2	15-6 (4.7)	16, 4.9
750,119.2	8, ½ (3.5, 0.2)	746, 118.6	15-6 (4.7)	24, 7.3

3.2.2 ASME Boiler and Pressure Vessel Code. Section VIII. Division 2 [15]

The Part 5 of this code provides the design-by-analysis requirements to evaluate complete stress analyses and prevent different failure modes to occur in equipment. The design-by-analysis rules use the results of numerical analysis to study plastic collapse, local failure, buckling collapse, and cyclic loading failure. Throughout this investigation, the author built detailed finite element models of API 12F shop welded tanks to determine the protection against failure from cyclic loading of these equipment, following the methods specified in the ASME BPVC.

The fatigue evaluations are made to estimate the number of applied cycles of stress that the equipment can resist before the collapse. The analysis can be developed using smooth bar or welded joint fatigue curves which are based on test specimens fabricated and inspected

according to the method presented in this code. The curves are essential to account for the allowable stress cycles in the equipment. Thus, in aboveground storage tanks, the cycles are usually produced by internal pressure or vacuum caused by the operation as well as any thermal condition related to the product contained.

The assessment procedure described in the ASME code recognizes that ratcheting might occur in the material of the equipment due to cycling loading. Hence, it provides specific guidance to evaluate protection against this condition. Moreover, the code requires to consider the effects of joint alignment and weld peaking in the fatigue evaluation.

This investigation performed an elastic stress analysis to carry out the fatigue assessment in the API 12F tanks. The method considers the primary plus secondary plus peak equivalent stress and an effective total equivalent stress amplitude to determine the permissible number of cycles of a specific tank model. A load history shall be identified according to the equipment operation, including any relevant time-dependent loading condition applied. Later, the stress tensor range and the range of primary plus secondary plus peak equivalent stress are computed at the evaluation point for a global pressure cycle using Equation (6) and Equation (7).

$$\Delta\sigma_{ij,k} = \left({}^{m}\sigma_{ij,k} - {}^{m}\sigma_{ij,k}^{LT}\right) - \left({}^{n}\sigma_{ij,k} - {}^{n}\sigma_{ij,k}^{LT}\right) \tag{6}$$

$$\Delta S_{p,k} = \frac{1}{\sqrt{2}}\Big[\left(\Delta\sigma_{11,k} - \Delta\sigma_{22,k}\right)^2 + \left(\Delta\sigma_{11,k} - \Delta\sigma_{33,k}\right)^2 + \left(\Delta\sigma_{22,k} - \Delta\sigma_{33,k}\right)^2 + 6\left(\Delta\sigma_{12,k} + \Delta\sigma_{13,k} + \Delta\sigma_{23,k}\right)^2\Big]^{0.5} \tag{7}$$

Where,

$\Delta\sigma_{ij,k}$ = stress tensor range

$\sigma_{ij,k}^{LT}$ = stress tensor due to local thermal stress

$\Delta S_{p,k}$ = range of primary plus secondary plus peak equivalent stress

m = start time point for the cycle

n = end time point for the cycle

Since varying thermal conditions were not considered in the fatigue analysis of the tanks, the stress tensor associated to this type of loading was neglected.

Using the range of primary plus secondary plus peak equivalent stress, the effective alternating equivalent stress can be computed from Equation (8) considering both a fatigue strength reduction factor and a fatigue penalty factor. Hence, while the fatigue strength reduction factor is related to the quality level on weld and surface conditions of the equipment, the fatigue penalty factor accounts the type of material and maximum temperature allowable in the cycles.

$$S_{alt,k} = \frac{K_f K_{e,k} \Delta S_{P,k}}{2} \tag{8}$$

Where,

K_f = fatigue strength reduction factor

$K_{e,k}$ = fatigue penalty factor

$S_{alt,k}$ = effective alternating equivalent stress

$\Delta S_{P,k}$ = range of primary plus secondary plus peak equivalent stress

The effective alternating equivalent stress is used to compute the number of design cycles following the procedure described in the Annex 3-F of the referred ASME code. The smooth bar design fatigue curves are polynomial functions that depend on the material

properties and the stress amplitude on the equipment. Equations (9)-(11) are provided to determine the number of permissible cycles.

$$N = 10^{X} \tag{9}$$

$$X = \frac{C_1 + C_3 Y + C_5 Y^2 + C_7 Y^3 + C_9 Y^4 + C_{11} Y^5}{1 + c_2 Y + C_4 Y^2 + C_6 Y^3 + C_8 Y^4 + C_{10} Y^5} \tag{10}$$

$$Y = \left(\frac{S_a}{C_{us}}\right)\left(\frac{E_{FC}}{E_t}\right) \tag{11}$$

Where,

C_1 ... C_{11} = material dependent constants

S_a = stress amplitude

C_{us} = conversion factor

E_{FC} = modulus of elasticity used to establish the design fatigue curve

E_t = modulus of elasticity of the material

3.3 Computational Models

The eleven (11) current API 12F shop-welded tanks and the two (2) proposed new sizes were modeled using the finite element software ABAQUS to estimate their fatigue life under normal operation cycles. Following the API 12F specification, the plate material used in the numerical analysis corresponds to an ASTM A36 [9] carbon steel. It was considered to be isotropic and elastic-plastic with a modulus of elasticity E = 2.9×10^7 psi (2.0×10^5 MPa), Poisson's ratio $\nu = 0.3$, and density $\rho = 490$ lb/ft^3 (7800 kg/m^3). In accordance with the API 650 [7], the minimum yield strength and allowable stress of the material were 36 ksi (250 MPa) and 23.2 ksi (160 MPa), respectively.

The FEA software ABAQUS version 6.13 [10] was used to build the tanks models and perform the stress analysis. Axisymmetric and 3D models were developed thorughout this investigation to evaluate the fatigue failure of the tanks. First, complete 3D models as shown in Figure 24 were analyzed using quadrilateral shell elements S4R to optimize the number of nodes in the models and decrease the simulation times. S4R elements are four-node, doubly curved elements with hourglass control, finite membrane strain, and reduced integration formulation. The mesh size was gradually reduced from the center of the tank to the top and bottom joints, in order to capture the stress values. From the analyses, it could be observed that the critical stresses due to internal pressure and vacuum occur at the top and bottom joints as well as at the sharp-corner between the semicircular top clean out and the bottom of the tanks.

In order to increase the precision in the analyses and have an accurate vision of the fatigue failure in the equipment, axisymmetric models of the API 12F shop welded tanks were built to analyze the stress concentrations at the roof-to-shell and shell-to-bottom joints far from the semicircular top clean-out. Four-node bilinear axisymmetric quadrilateral elements (CAX4R) with reduced integration and hourglass control were used in the analysis to capture the stresses and displacements of the models. A mesh size of 1/32 in. (0.8 mm) was assigned throughout the sections of the tanks, after a mesh adaptivity analysis was carried out to study the convergence of the results. Figure 25 shows the typical welded joints of the API 12F axisymmetric tank models.

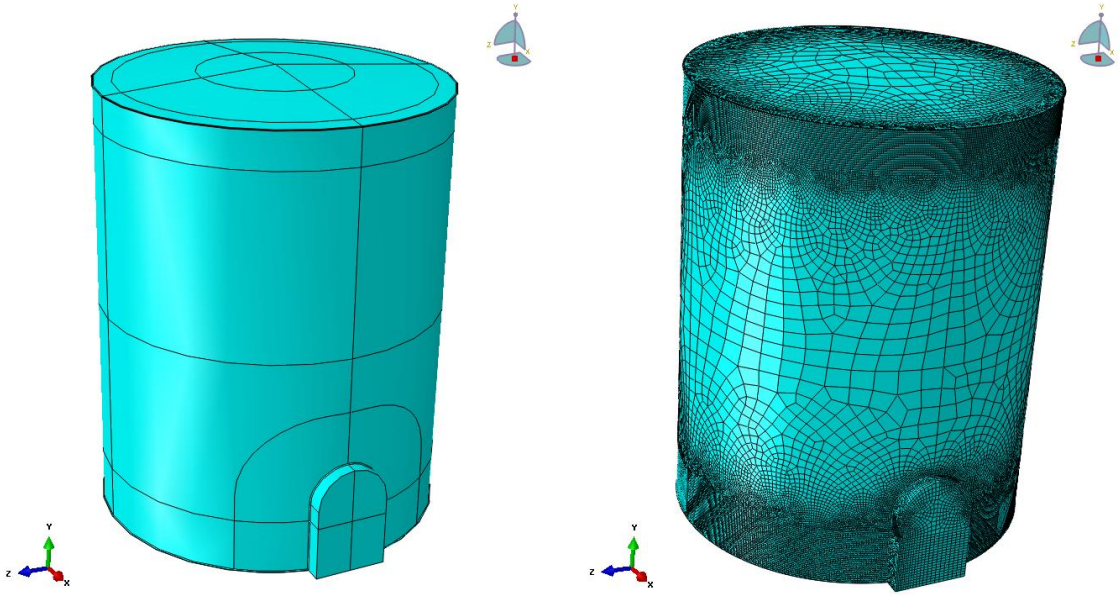

Figure 24. Typical API 12F finite element tank 3D model.

Moreover, finite element submodels were created using the complete 3D tank models to study the stress concentrations located between the clean-out and the bottom of the equipment. Submodeling is a technique commonly used to improve the accuracy of the analysis in high stress areas, the calculations are carried out based on the interpolation of results already obtained from a global model. Thus, the displacements obtained from the global tank models were applied as boundary conditions in the submodels. Figure 26 shows a typical submodel of the juncture between the clean-out and the tank bottom. Three-dimensional solid ten-node quadratic tetrahedron elements (C3D10) were used in the submodels to obtain the stress and displacements results from the analysis. Furthermore, an adaptivity analysis was implemented along with five iterations to refine the mesh close to the stress concentrations. However, since the studied juncture is a sharp-corner between two different steel plates, the extrapolation method proposed by Niemi et al [11] was used to the obtain the results and avoid the stress singularities. This method provides specific

meshing guidelines to be followed in order to evaluate the stresses near a structural discontinuity. Three strain gauges shall be defined at locations 0.4t, 0.9t, and 1.4t from the weld toe. Thus, the structural stress at the juncture can be determined by extrapolation of the stress components using Equation (12).

$$\sigma_c = 2.52\,\sigma_{0.4t} - 2.24\,\sigma_{1.0t} + 0.72\,\sigma_{1.4t} \quad (12)$$

Where σ_c is a stress component at the intersection point, $\sigma_{0.4t}$, $\sigma_{0.9t,}$ and $\sigma_{1.4t}$ are the corresponding stress components at locations 0.4t, 0.9t, and 1.4t, and t is the bottom thickness. After finding the stress components, the principal stresses shall be computed to obtain the equivalent stress using Equation (5).

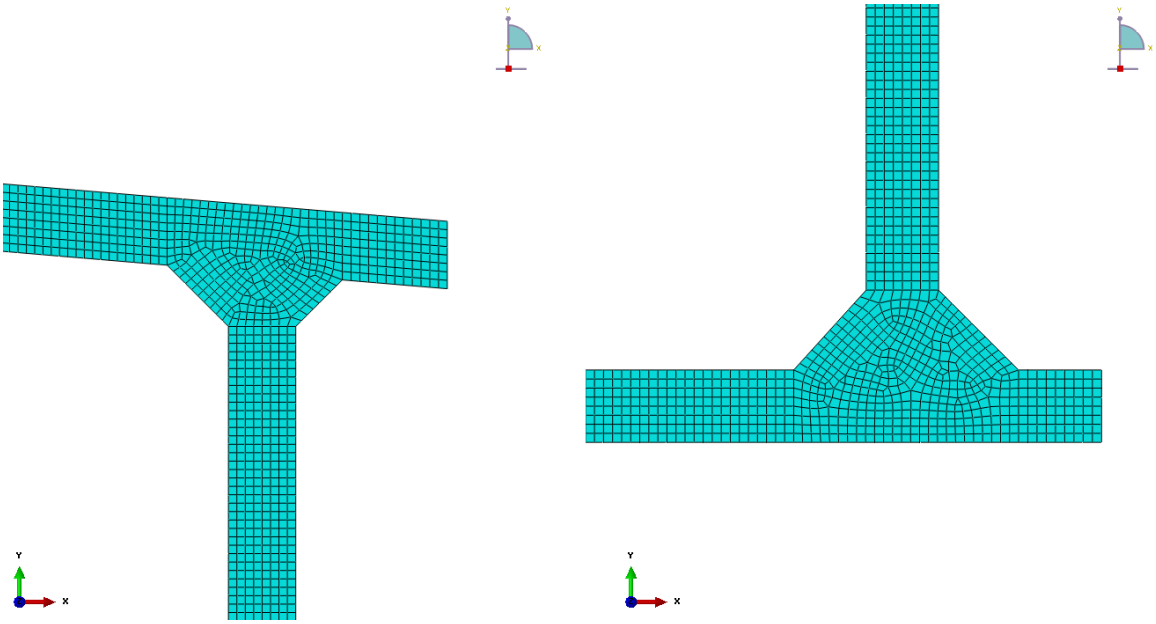

Figure 25. Typical welded joints of the API 12F axisymmetric tank models

The fatigue evaluation was performed considering the normal operation of the equipment. Thus, the fatigue cycles were defined using specific design internal pressures and vacuum pressures. According to their diameter, the tank models were separated in three groups and

different pressure cycles were assigned for the analysis. First, for tanks 7 ft. 11 in. (2.4 in) to 11 ft. (3.4 m) diameter, the cycles consisted in design pressure of 24 oz/in^2 (10.3kPa) and vacuum pressure of 0.5 oz/in^2 (0.2 kPa). Second, for tanks 12 ft. (3.7 m) diameter, the cycles consisted in design pressure of 16 oz/in^2 (6.9 kPa) and vacuum pressure of 0.5 oz/in^2 (0.22 kPa). Finally, for tanks 15 ft. 6 in. (4.7m) diameter or larger, the cycles consisted in design pressure of 8 oz/in^2 (3.4 kPa) and vacuum pressure of 0.5 oz/in^2 (0.2 kPa). The tanks were considered with 18 in. (0.45 m) of liquid product using a specific gravity of 0.7 and the design temperature for the fatigue evaluation was taken as ambient temperature, 70° F (21° C).

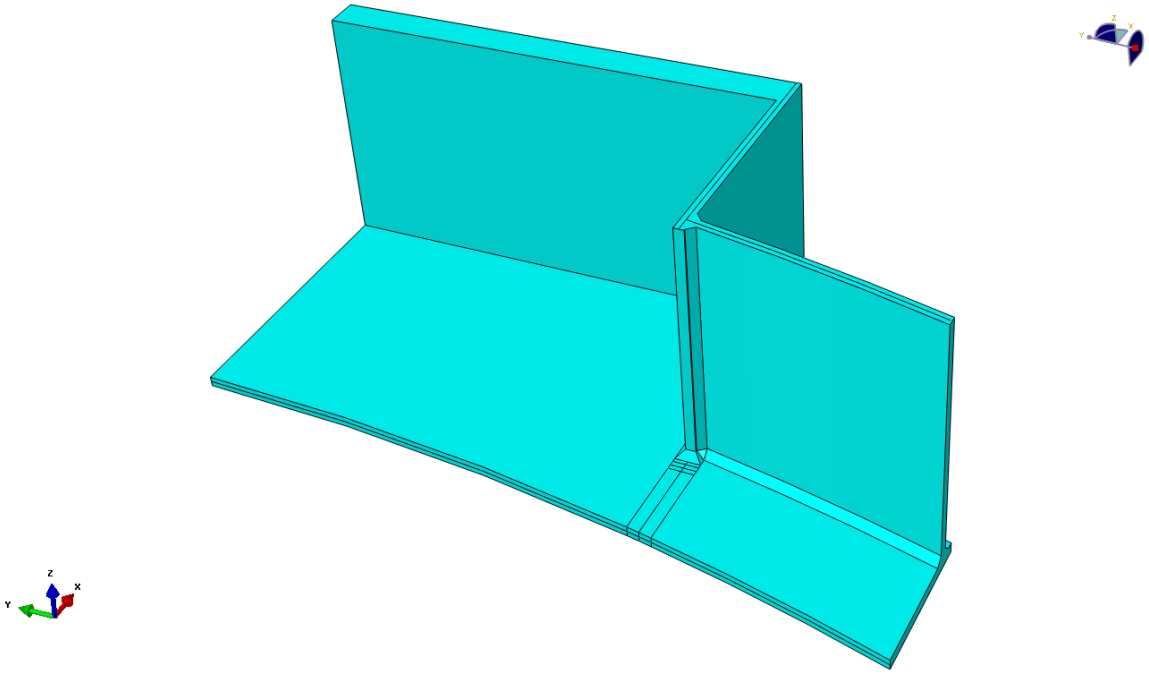

Figure 26. Typical submodel of the intersection between the clean-out and the tank bottom.

The API 12F requires specific bottom and shell thicknesses to ensure structural integrity of the tanks and the minimum plate thickness cannot be decreased in any case. Hence, the

bottom and shell thicknesses of the models were assigned considering the tank diameters and the three different groups mentioned before. Thus, a 3/16 in. (4.8 mm) shell and 1/4 in. (6.4 mm) bottom were used for the small diameter group, 1/4 in. (6.4 mm) shell and 1/4 in. (6.4 mm) bottom were used for the medium diameter group, and a 1/4 in. (6.4 mm) shell and 3/8 in. (9.5 mm) bottom were used for the large diameter group. As stated in the API 12F, the roof plates have the same the thickness as the shell plates. Table 12 summarized the pressure cycles and thicknesses assigned to each tank model.

Table 12. Summary of pressure cycles and thicknesses in the tank models.

	Pressure Cycle (oz/in², kPa)		**Diameter ft, in (m)**	**Height ft, m**	**Shell Thickness in, mm**	**Bottom Thickness in, mm**
	Design Pressure	**Vacuum Pressure**				
Case 1	24, 10.3	0.5, 0.2	7-11 (2.4)	10, 3.0	3/16, 4.8	1/4, 6.4
Case 2	24, 10.3	0.5, 0.2	9-6 (2.9)	8, 2.4	3/16, 4.8	1/4, 6.4
Case 3	24, 10.3	0.5, 0.2	9-6 (2.9)	12, 3.7	3/16, 4.8	1/4, 6.4
Case 4	16, 6.9	0.5, 0.2	12-0 (3.7)	10, 3.0	1/4, 6.4	1/4, 6.4
Case 5	24, 10.3	0.5, 0.2	10-0 (3.0)	15, 4.6	3/16, 4.8	1/4, 6.4
Case 6	24, 10.3	0.5, 0.2	11-0 (3.4)	15, 4.6	3/16, 4.8	1/4, 6.4
Case 7	16, 6.9	0.5, 0.2	12-0 (3.7)	15, 4.6	1/4, 6.4	1/4, 6.4
Case 8	16, 6.9	0.5, 0.2	12-0 (3.7)	20, 6.1	1/4, 6.4	1/4, 6.4
Case 9	16, 6.9	0.5, 0.2	12-0 (3.7)	25, 7.6	1/4, 6.4	1/4, 6.4
Case 10	8, 3.4	0.5, 0.2	15-6 (4.7)	16, 4.9	1/4, 6.4	3/8, 9.5
Case 11	8, 3.4	0.5, 0.2	15-6 (4.7)	24, 7.3	1/4, 6.4	3/8, 9.5
Case 12	8, 3.4	0.5, 0.2	15-6 (2.4)	30, 9.1	1/4, 6.4	3/8, 9.5
Case 13	8, 3.4	0.5, 0.2	21-6 (2.9)	16, 4.9	1/4, 6.4	3/8, 9.5

The soil-structure interaction was considered by using linear elastic springs in the bottom of the tank models acting in vertical direction. In this way, only compression springs were utilized in the analysis. An iterative method was employed to remove all the springs in tension after applying the design pressure. Moreover, it was observed that the vacuum pressure produced the tanks bottom to settle. Therefore, several configurations were

considered in the analysis to support the tanks base. Compacted sand soil, reinforced concrete pad, and a combination of sand soil under the tank bottom with concrete ringwalls under the tank shell were studied to determine the most conservative support condition for the tank models. Finally, the properties of a compacted sand soil were utilized in the analysis and subgrade modulus of 250 lbf/in^3 (68000 kN/m^3) [8] was assigned to the springs stiffness to represent the soil material.

3.4 Fatigue Evaluation - Elastic Stress Analysis

The stress analysis was performed following the ASME design-by-analysis rules mentioned in Section 3.2.2. The stress components were obtained from the results using ABAQUS and the stress tensor range and the range of primary plus secondary plus peak equivalent stress were computed using Equations (6) and (7).

As mentioned before, the effective alternating equivalent stress is defined as one-half of the effective total equivalent stress range multiplied by a fatigue penalty factor and a fatigue strength reduction factor. In order to obtain the fatigue penalty factor as well as carry out the ratcheting analysis, the primary plus secondary equivalent stress range had to be computed. Thus, a linearization of the results was made to categorize the stresses and the primary plus secondary equivalent stress range was computed as directed in the ASME code. For the axisymmetric models, the linearization was made in different stress classification lines (SCL) across the roof-to-shell and shell-to-bottom joints of the tanks as shown in Figure 27. Both the inside and outside points of the SCL were studied and the fatigue life of the tanks were estimated according to the alternating stresses obtained in these points. Figure 28 shows a typical stress classification for a cross section of the tank

models. For the solid submodels, the stress linearization of the stress components was performed in a cross-section of the tanks bottom along the partitions located at 0.4*t*, 0.9*t*, and 1.4*t* from the weld toe. Hence, the results were extrapolated to find the stress components at the intersection points and compute the primary plus secondary equivalent stress range.

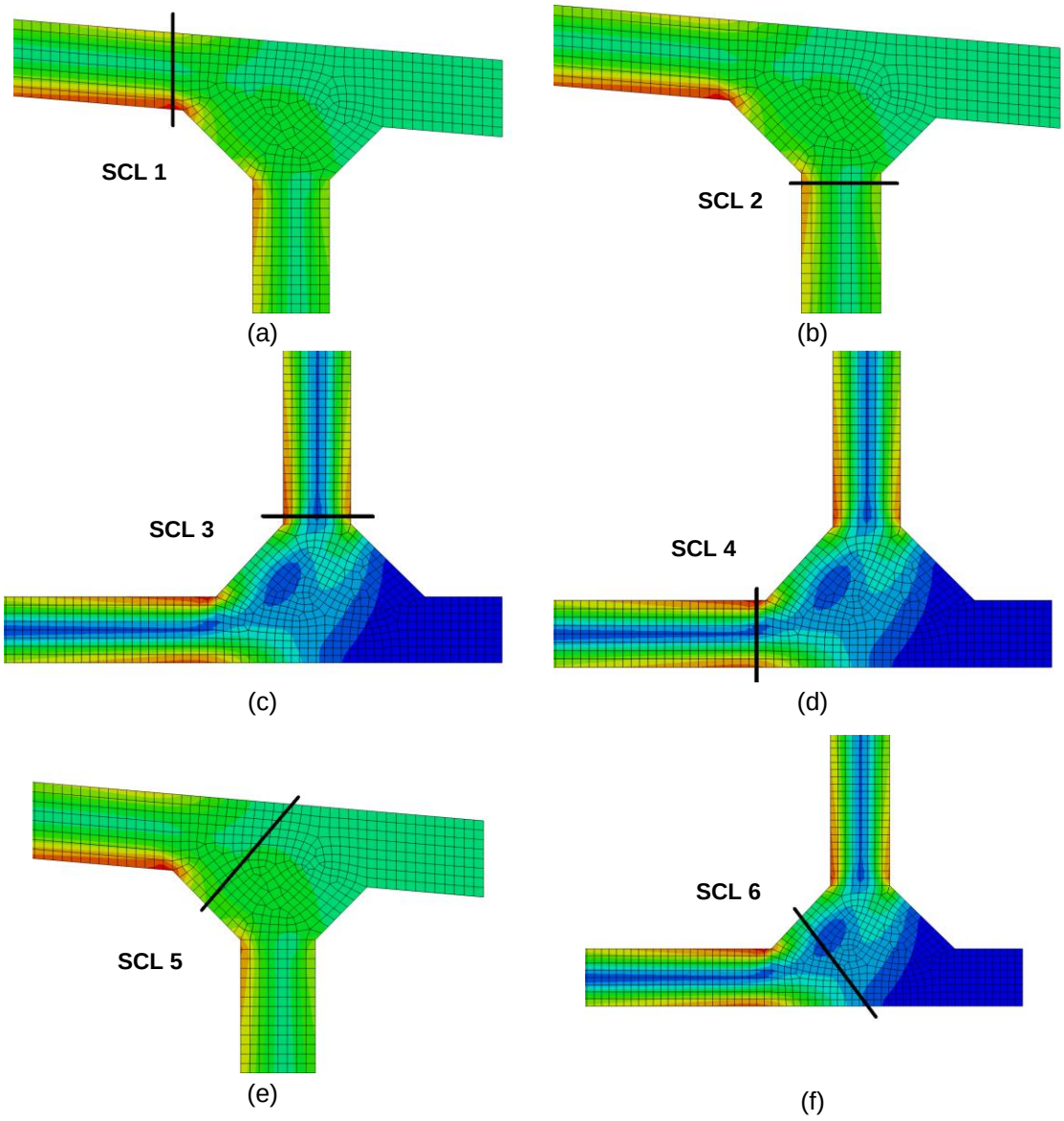

Figure 27. Stress Classification Lines

In cases where the primary plus secondary equivalent stress ranges were smaller than the allowable limit, the protection against ratcheting was checked and the assigned fatigue penalty factor, $K_{e,k}$, was equal to 1.0 for the fatigue evaluation. However, if the primary plus secondary equivalent stress ranges were larger than the allowable limit, the fatigue penalty factor, $K_{e,k}$, was computed in accordance with the ASME formulation. The material constants *m* and *n* for carbon steel were 3.0 and 0.2, respectively.

The fatigue strength reduction factor depends on the type of welding and surface finish of the tanks as well as the examination done to the welds. The roof-to-shell and shell-to-bottom joints consisted of fillet welds, both inside and outside. It was assumed for the evaluation points along SCL 1 to 4 located at the toe that the welds only received VT examination (visual), and for the evaluation points along SCL 5 and 6 located at the backside of the fillet welds, the welds received no examination. Therefore, the assigned fatigue strength reduction factor for SCL 1 to 4 was K_f, = 2.5 and for SCL 5 to 6, K_f, = 4.0 as stated in Table 5.12 from the ASME Boiler and Pressure Vessel Code [15].

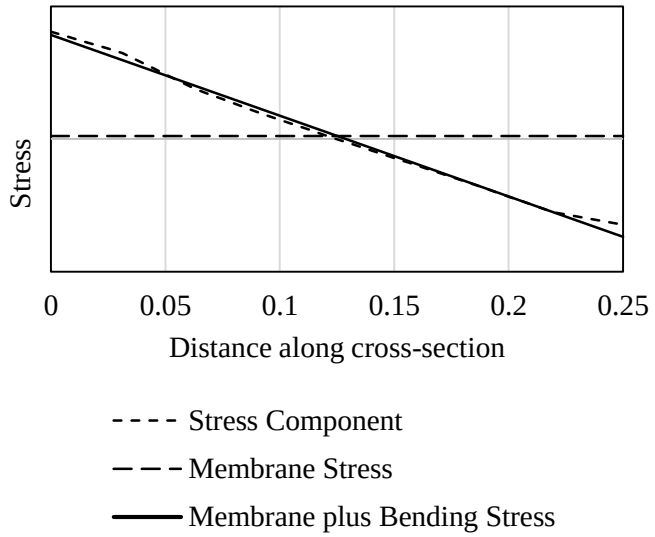

Figure 28. Typical stress classification for a cross section

After computing the effective alternating equivalent stress, the number of permissible cycles was obtained using Equation (9). These results were compared to the S-N curves provided in the ASME Boiler and Pressure Vessel Code, Section VIII, Division 2, 2004 Edition. The 2004 edition was the last one that included the design fatigue curves for different materials instead of providing the formulation to compute the number of cycles. This procedure was carried out to check the validity of the results. A smooth bar design fatigue curve obtained by following the formulation presented in the Annex 3-F of the ASME code is shown in Figure 29.

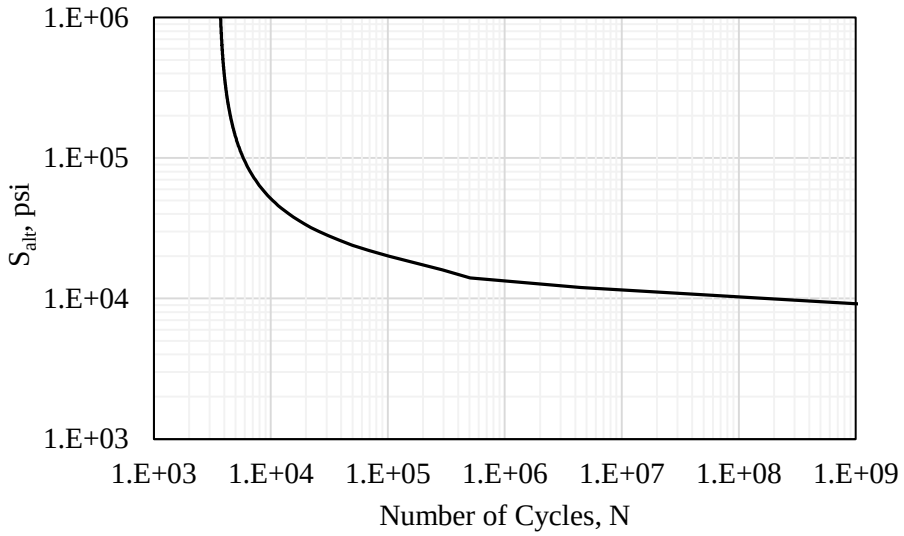

Figure 29. Smooth bar design fatigue curve for Carbon, Low Alloy, Series 4xx, and High Tensile Strength Steels for temperatures not exceeding 371°C (700°F) where $6_{uts} \leq$ 80 Ksi (552 MPa)

The permissible pressure cycles obtained after evaluating the top and bottom joints using axisymmetric models of each API 12F tank are presented in Table 13. It can be observed that the number of allowable cycles obtained from the SCL 1 and 2 do not increase with the height of the tanks. However, the stress classification lines at the shell-to-bottom joint (SCL 3 and 4) indicate that tanks with smaller height tend to have a shorter fatigue life than tanks with larger height. Moreover, for tanks with 11 ft (3.4 m) diameter or smaller, the allowable number of pressure cycles was dictated from the behavior of the shell-to-bottom joints instead of the roof-to-shell joints as recommended by the API 937 for storage tanks with frangible roof joint. It is also important to note that the inside evaluation points reflected less number of permissible cycles than the outside points.

The pressure cycles computed after the evaluation of stresses in the joint between the clean-out attachment and the tank base using solid submodels and the extrapolation method are

presented in Table 14. From the results, it can be noted that tanks with smaller diameters allow less pressure cycles than tanks with larger diameters. Moreover, the groups of tanks with 12 ft. (3.7 m) diameter demonstrated that the selfweight of the shell reduces the deformation and equivalent stress range produced in the clean out joint due to internal pressure and vacuum, increasing the permissible pressure cycles. Finally, comparing the number of cycles computed after evaluating the top and bottom joints as well as the clean-out joint, the minimum allowable cycles for each API 12F is presented in Figure 30.

Table 13. Number of permissible cycles at the top and bottom joints of API 12F shop welded tanks

Case	Pressure Cycle (oz/in², kPa)		SCL 1 (Cycles)		SCL 2 (Cycles)		SCL 3 (Cycles)		Min number of cycles
	Design Pressure	Vacuum Pressure	Inside Point	Outside Point	Inside Point	Outside Point	Inside Point	Outside Point	
1	24, 10.3	0.5, 0.2	1.5E+05	4.0E+05	1.9E+05	5.6E+05	**4.8E+04**	5.9E+04	**4.8E+04**
2	24, 10.3	0.5, 0.2	3.1E+04	9.5E+04	5.2E+04	1.4E+05	**1.4E+04**	1.5E+04	**1.4E+04**
3	24, 10.3	0.5, 0.2	3.1E+04	9.5E+04	5.3E+04	1.4E+05	**1.7E+04**	1.9E+04	**1.7E+04**
4	16, 6.9	0.5, 0.2	**1.8E+05**	1.9E+06	3.6E+05	4.1E+06	3.5E+05	4.8E+05	**1.8E+05**
5	24, 10.3	0.5, 0.2	3.3E+04	1.0E+05	5.4E+04	1.5E+05	**2.5E+04**	3.2E+04	**2.5E+04**
6	24, 10.3	0.5, 0.2	2.3E+04	5.9E+04	3.4E+04	7.8E+04	**1.7E+04**	2.1E+04	**1.7E+04**
7	16, 6.9	0.5, 0.2	**1.8E+05**	1.9E+06	3.6E+05	4.2E+06	4.9E+06	2.3E+07	**1.8E+05**
8	16, 6.9	0.5, 0.2	**1.8E+05**	1.9E+06	3.6E+05	4.1E+06	1.2E+09	6.5E+09	**1.8E+05**
9	16, 6.9	0.5, 0.2	**1.8E+05**	1.9E+06	3.6E+05	4.1E+06	1.6E+11	3.3E+11	**1.8E+05**
10	8, 3.4	0.5, 0.2	**5.3E+05**	2.1E+08	3.7E+06	3.9E+08	1.3E+07	1.5E+06	**5.3E+05**
11	8, 3.4	0.5, 0.2	**5.3E+05**	2.1E+08	3.8E+06	3.9E+08	2.9E+08	2.6E+07	**5.3E+05**
12	8, 3.4	0.5, 0.2	**6.1E+05**	2.1E+08	3.7E+06	3.9E+08	9.0E+06	1.1E+06	**6.1E+05**
13	8, 3.4	0.5, 0.2	**6.3E+04**	2.8E+05	9.9E+04	2.5E+05	1.4E+10	5.9E+10	**6.3E+04**

Case	Pressure Cycle (oz/in², kPa)		SCL 3 (Cycles)		SCL 4 (Cycles)		SCL 5 (Cycles)		Min number of cycles
	Design Pressure	Vacuum Pressure	Inside Point	Outside Point	Inside Point	Outside Point	Inside Point	Outside Point	
1	24, 10.3	0.5, 0.2	2.2E+05	4.4E+05	1.4E+05	1.5E+06	4.3E+05	2.6E+11	**4.8E+04**
2	24, 10.3	0.5, 0.2	1.5E+04	1.6E+04	2.9E+04	6.8E+04	3.7E+04	1.9E+05	**1.4E+04**
3	24, 10.3	0.5, 0.2	4.3E+04	7.5E+04	4.2E+04	2.0E+05	8.0E+04	2.3E+08	**1.7E+04**
4	16, 6.9	0.5, 0.2	2.0E+05	4.6E+05	2.5E+05	7.6E+07	5.3E+07	2.8E+08	**1.8E+05**
5	24, 10.3	0.5, 0.2	7.4E+04	2.2E+05	4.3E+04	2.0E+05	1.2E+05	9.5E+10	**2.5E+04**
6	24, 10.3	0.5, 0.2	4.1E+04	1.1E+05	2.9E+04	1.0E+05	5.8E+04	1.9E+09	**1.7E+04**
7	16, 6.9	0.5, 0.2	8.9E+05	2.6E+07	2.5E+05	7.6E+07	1.8E+10	*	**1.8E+05**
8	16, 6.9	0.5, 0.2	3.6E+08	3.4E+09	2.5E+05	7.3E+07	2.7E+11	*	**1.8E+05**
9	16, 6.9	0.5, 0.2	1.1E+11	3.2E+11	3.6E+05	7.6E+07	7.7E+08	*	**1.8E+05**
10	8, 3.4	0.5, 0.2	*	*	9.1E+05	5.5E+09	*	*	**5.3E+05**
11	8, 3.4	0.5, 0.2	*	*	4.1E+06	6.4E+09	*	*	**5.3E+05**
12	8, 3.4	0.5, 0.2	*	*	9.2E+05	1.7E+11	*	*	**6.1E+05**
13	8, 3.4	0.5, 0.2	*	*	7.5E+04	4.7E+05	1.1E+07	*	**6.3E+04**

* Stress was too small to obtain an accurate result.

Table 14. Number of allowable pressure cycles at clean-out joints of API 12F shop welded flat bottom tanks

	Pressure Cycle (oz/in², kPa)		Diameter ft, in (m)	Height ft, m	Minimum number of cycles
	Design Pressure	**Vacuum Pressure**			
Case 1	24, 10.3	0.5, 0.2	7, 11 (2.4)	10, 3.0	**2.3E+04**
Case 2	24, 10.3	0.5, 0.2	9, 6 (2.9)	8, 2.4	**4.0E+03**
Case 3	24, 10.3	0.5, 0.2	9, 6 (2.9)	12, 3.7	**7.2E+03**
Case 4	16, 6.9	0.5, 0.2	12, 0 (3.7)	10, 3.0	**9.0E+03**
Case 5	24, 10.3	0.5, 0.2	10, 0 (3.0)	15, 4.6	**6.2E+03**
Case 6	24, 10.3	0.5, 0.2	11, 0 (3.4)	15, 4.6	**4.8E+03**
Case 7	16, 6.9	0.5, 0.2	12, 0 (3.7)	15, 4.6	**1.5E+04**
Case 8	16, 6.9	0.5, 0.2	12, 0 (3.7)	20, 6.1	**2.3E+04**
Case 9	16, 6.9	0.5, 0.2	12, 0 (3.7)	25, 7.6	**4.7E+04**
Case 10	8, 3.4	0.5, 0.2	15, 6 (4.7)	16, 4.9	**6.7E+07**
Case 11	8, 3.4	0.5, 0.2	15, 6 (4.7)	24, 7.3	**1.4E+08**
Case 12	8, 3.4	0.5, 0.2	7, 11 (2.4)	10, 3.0	**8.5E+06**
Case 13	8, 3.4	0.5, 0.2	9, 6 (2.9)	8, 2.4	**8.4E+04**

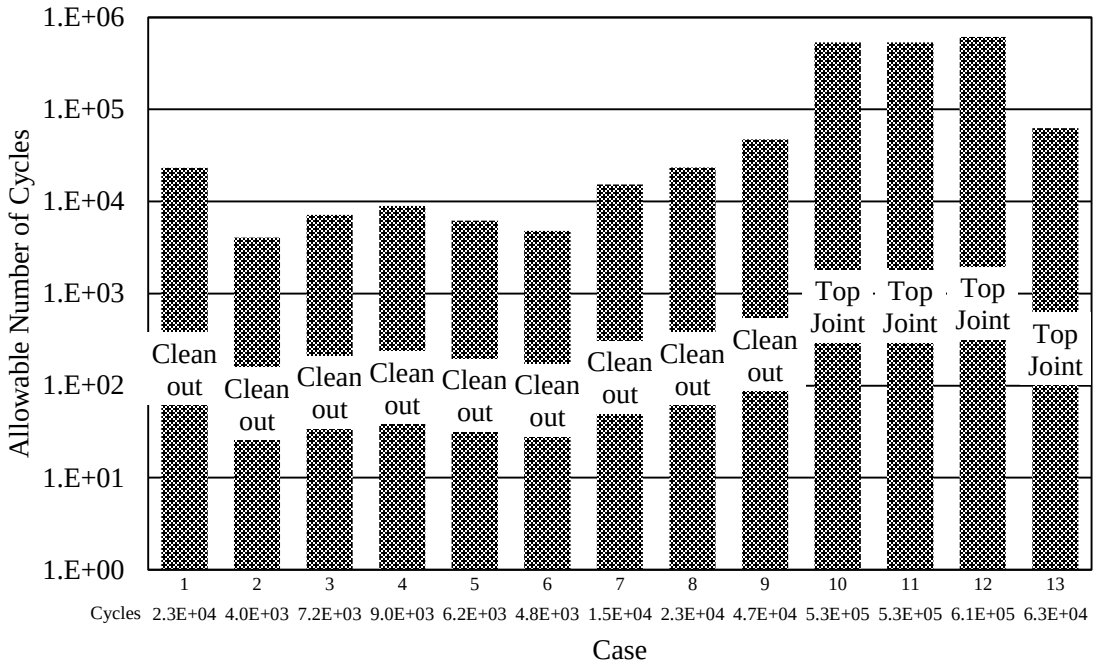

Figure 30. Minimum number of cycles for each API 12F tank and location of the most critical joint.

3.5 Conclusions

An elastic stress analysis was performed to study fatigue life of the API 12F shop-welded tanks in accordance with the ASME Boiler and Pressure Vessel Code. Section VIII. Division 2, 2013 Edition. Three different joints were evaluated throughout this research: the roof-to-shell joint, the shell-to-bottom joint and the clean-out intersection with the tank bottom. While axisymmetric models were built to study the first two joints, 3D solid submodels were constructed to determine the allowable number of pressure cycles in the clean-out juncture. This study yields the following conclusions:

- The permissible number of pressure cycles was determined and summarized in Figure 30. The most critical API 12F storage tank in terms of fatigue evaluation was the Case 2 (9 ft 6 in (2.9 m) diameter and 8 ft (2.4 m) high) which allows approximately four thousand cycles.
- The evaluation of the three referred joints proved that the height of the tank and the selfweight of the shell increase the number of permissible cycles especially in tanks with smaller diameter (12 ft (3.7 m) or less) because they reduce the deformation at the bottom of the equipment.
- The analysis of top and bottom joints using axisymmetric models revealed that for tanks with 12 ft (3.7 m) diameter or smaller, the shell-to-bottom joint has a shorter fatigue life than the roof-to-shell joint. Hence, the fatigue analysis estimated that the bottom of the tanks fail prior to the top joint, producing an oil spillage hazard.
- The study of the clean out juncture to the base of the tanks determined that this intersection is critical in the fatigue life of API 12F tanks with 12ft (3.7m) diameter

and smaller. For the tanks 15ft. 6in. (4.7 m) diameter or larger, the behavior of the top joint was more significant in the estimation of permissible pressure cycles.

CHAPTER 4. CONCLUSION

4.1 Failure Pressure of the API 12F Storage Tanks

Various failure pressure modes were study throughout this investigation, the yielding pressure of each API 12F tank model was determined using an elastic stress analysis. In general, the storage tanks failed at the top joint before yielding occur at the bottom joint. Only five cases did not ensure the frangible roof joint behavior representing a hazard if these tanks are subjected to overpressure. Additionally, yielding pressure obtained from the finite element analysis of the tanks was always greater than the pressure computed using the API 937 formulation.

Even though the estimation of the uplift deformations calculated using FEA and the API 937 or API 650 formulations resulted in similar results, the FE models showed that the API 650 uplift criteria might be too conservative to the API 12F shop-welded tanks. The equipment were capable of resisting further internal pressure after some uplift occurred at the base.

The design pressure for the studied tanks was raised up to 24 oz/in^2 (10.3 kPa), which did not cause failure in any tank top or bottom joints. However, significant uplift deformations were observed in the group of tanks with 15ft. 6in diameter and larger. Further investigation is recommended to determine if the increase in the design pressure might affect the safety of the equipment.

In general, the elastic buckling analysis showed that the buckling pressures of the API 12F tanks are greater than the yielding pressures. Only the tank models with 21ft. 6in diameter presented some buckling before the yielding failure occurred at the top joint.

The elastic-plastic stress analysis evaluated the plastic collapse of the equipment. It was observed that rupture occurred at the top joint of the tanks in all the cases studied. Moreover, the rupture-to-yielding ratios ranged from 1.4 to 6.4

Additionally, rupture at the intersection of the clean-out with the tank bases was observed in the elastic-plastic analysis of the models. Thus, a fatigue analysis was recommended and addressed in Chapter 3 of this document.

The wind load analysis indicated low stress levels and small uplift deformations. It was concluded that the wind pressure was not critical in the analysis of the tank failure modes.

4.2 Fatigue Analysis of the API 12F Tanks

The fatigue evaluation was developed using an elastic stress analysis of the API 12F tanks. The allowable number of pressure cycles were estimated by analyzing three critical joints in the tank models: the roof-to-shell joint, the shell-to-bottom joint, and the intersection between the clean-out and the tank bottom. The first two joints were modeled with axisymmetric models and the third one was analyzed with solid elements and using submodeling techniques.

It was observed that for tanks with a diameter of 12ft and smaller, the clean-out intersection presented a shorter fatigue life than the other junctures. On the other hand, tanks with a 15ft. 6in diameter and larger showed that the most critical joint in terms of permissible pressure cycles was the roof-to-shell joint.

LIST OF REFERENCES

LIST OF REFERENCES

[1] API 12F, Specification for shop welded tanks for storage of production liquids, Twelfth Edition. Washington, D.C.: American Petroleum Institute; 2008.

[2] Myers, P. E. Aboveground storage tanks. Vol. 690. McGraw-Hill, 1997.

[3] Jaca, R C., and Godoy L A., Wind buckling of metal tanks during their construction. Thin-Walled Structures, 2010; 48.6: 453-459.

[4] Drogaris, G. K. Major accidents in oil and gas industries. SPE Health, Safety and Environment in Oil and Gas Exploration and Production Conference. Society of Petroleum Engineers, 1991.

[5] API 937, Evaluation of design criteria for storage tanks with frangible roof joints. Washington, D.C.: American Petroleum Institute; 1996.

[6] Lu, Zhi. Evaluation of design criteria for storage tanks with frangible roof joints. Diss. Kansas State University, 1994.

[7] API 650, Welded tanks for oil storage, Twelfth Edition. Washington, D.C.: American Petroleum Institute; 2013.

[8] Swenson, D., Fenton, D., Lu, Z., Ghori, A., and Baalman, J., Evaluation of Design Criteria for Storage Tanks with Frangible Roof Joints, Welding Research Council Bulletin 410, ISSN 0043-2326, Welding Research Council, United Engineering Center, 345 East 47th Street, New York, NY, 10017, April, 1996.

[9] ASTM A36. Standard Specification for Carbon Structural Steel. 2008.

[10] ABAQUS. Abaqus Analysis User's Manual version 6.13. Providence, RI: Dassault Systemes Simulia Corp.; 2013.

[11] Niemi, E., Fricke, W., Maddox, S.J., Fatigue analysis of welded joints - Designer's guide to the structural hot-spot stress approach, IIW Doc IIW-1430-00, Cambridge, Woodhead: International Institute of Welding; 2006

[12] Ellobody, E., Feng R., and Young B. Finite Element Analysis and Design of Metal Structures. Elsevier, 2013.

[13] Wang, J. H., and A. Koizumi. Buckling of cylindrical shells with longitudinal joints under external pressure. Thin-Walled Structures 2010; 48.12: 897-904.

[14] API 579-1/ASME FFS-1, Fitness-For-Service, Second Edition. Washington, D.C.: American Petroleum Institute; 2007.

[15] ASME Boiler and Pressure Vessel Code, Section VIII. Alternative rules for construction of pressure vessels, Division 2. New York, NY: American Society of Mechanical Engineers; 2013.

[16] Riks, E., An incremental approach to the solution of snapping and buckling problems. Int. J. Solids & Struct. 1979; 15(7):529-551.

[17] Maraveas, C., Balokas, G. A., and Tsavdaridis, K. D. Numerical evaluation on shell buckling of empty thin-walled steel tanks under wind load according to current American and European design codes. Thin-Walled Structures 2015; 95: 152-160.

[18] Zhao, Y., and Lin, Y. Buckling of cylindrical open-topped steel tanks under wind load. Thin-Walled Structures, 2014 79: 83-94.

[19] Zhao, Y., Cao, Q. S., and Su, L. Buckling design of large circular steel silos subject to wind pressure. Thin-Walled Structures, 2013; 73: 337-349.

[20] Prinz, GS, and Nussbaumer A. Fatigue analysis of liquid-storage tank shell-to-base connections under multi-axial loading. Engineering Structures 2012, 40: 75-82

[21] Prinz, GS, and Nussbaumer A. On the low-cycle fatigue capacity of unanchored steel liquid storage tank shell-to-base connections. Bulletin of Earthquake Engineering, 2012: 10.6: 1943-1958.

[22] Ahari MN, Eshghi S, Ashtiany MG. The tapered beam model for bottom plate uplift analysis of unanchored cylindrical steel storage tanks. Engineering Structures 2009; 31:623–32.

[23] Malhotra PK, Veletsos AS. Uplifting analysis of base plates in cylindrical tanks. Journal of Structural Engineering 1994; 120(12):3489–505.

[24] Malhotra PK. Base uplifting analysis of flexibly supported liquid-storage tanks. Earthquake engineering & structural dynamics 1995; 24:1591–607.

PUBLICATIONS

PUBLICATIONS

Journal Papers:

Rondon A, Guzey S. Determination of localized stresses in the shell above anchor bolt chairs attachments of anchored storage tanks. Thin-Walled Structures 2016; 98: 617-626.

Rondon A, Guzey S. Failure Pressure of the API Specification 12F Shop Welded, Flat Bottom Tanks. Thin-Walled Structures. (Paper Submitted)

Conference Proceedings

Rondon A, Guzey S. Evaluation of the Anchor-Bolt Chair Design Considering Localized Stresses in the Shell of Anchored Storage Tanks. ASME 2016 Pressure Vessels and Piping Conference. (Final Paper Submitted)

Rondon A, Guzey S. Evaluation of the Design Pressure and Failure modes for the API 12F Shop Welded Flat Bottom Tanks for oil storage. ASME 2016 Pressure Vessels and Piping Conference. (Final Paper Submitted)